sustainability

MDPI

Review

Parameter Extraction of Solar Photovoltaic Cell and Module Models with Metaheuristic Algorithms: A Review

Zaiyu Gu [1], Guojiang Xiong [1,2,*] and Xiaofan Fu [1]

[1] College of Electrical Engineering, Guizhou University, Guiyang 550025, China
[2] Guizhou University Institute of Engineering Investigation and Design Co., Ltd., Guiyang 550025, China
* Correspondence: gjxiongee@foxmail.com

Abstract: As the photovoltaic (PV) market share continues to increase, accurate PV modeling will have a massive impact on the future energy landscape. Therefore, it is imperative to convert difficult-to-understand PV systems into understandable mathematical models through equivalent PV models. However, the multi-peaked, non-linear, and strongly coupled characteristics of PV models make it challenging to extract accurate parameters of PV models. Metaheuristics can address these challenges effectively regardless of gradients and function forms, and have gained increasing attention in solving this issue. This review surveys different metaheuristics to the PV model parameter extraction and explains multiple algorithms' behavior. Some frequently used performance indicators to measure the effectiveness, robustness, accuracy, competitiveness, and resources consumed are tabulated and compared, and then the merits and demerits of different algorithms are outlined. The patterns of variation in the results extracted from different external environments were analyzed, and the corresponding literature was summarized. Then, challenges for both metaheuristics and application scenarios are analyzed. Finally, corresponding perspectives on future research are summarized as a valid reference for technological advances in PV model parameter extraction.

Keywords: PV model; parameter extraction; metaheuristic

Citation: Gu, Z.; Xiong, G.; Fu, X. Parameter Extraction of Solar Photovoltaic Cell and Module Models with Metaheuristic Algorithms: A Review. *Sustainability* **2023**, *15*, 3312. https://doi.org/10.3390/su15043312

Academic Editors: Luis Hernández-Callejo, Prince Winston David and Praveen Kumar B

Received: 6 January 2023
Revised: 2 February 2023
Accepted: 7 February 2023
Published: 10 February 2023

1. Introduction

Fossil fuels' total reserves are limited, and their overuse has threatened human health and the ecological environment. Thus, developing renewable energy sources is an extremely urgent concern [1–5]. Renewable energy, including the energy sources of solar, hydro, wind, geothermal, and biomass energy [6–8], is inexhaustible or short-term renewable. Solar energy is a form of energy that contains a tremendous amount of energy and has the potential to meet all the energy requirements of current human activities [9]. As a result, solar energy has been employed in varied applications such as desalination, heating plants, and photovoltaic (PV) power generation [10,11]. Due to the clean and widespread availability of electrical energy in various fields, PV power generation is an important project for developing renewable energy sources [12].

Accurate modeling is essential for the assessment, efficiency improvement, fault analysis, and simulation of PV systems [13–15]. A PV system consists of an aggregation of PV cells, and they are typically modeled with equivalent circuits, mainly including single diode (SDM), double diode (DDM), and triple diode (TDM) models [16–18]. These equivalent circuits can simulate PV cells' electrical characteristics. They have five, seven, and nine parameters to be extracted, respectively. As the number of diodes increases, more parameters to be extracted are involved, which results in more computational difficulty. The challenges faced by the issue include not only the multiplication of solution complexity due to multiple unknown parameters but also the coupling between electrical quantities, leading to a highly implicit function [4,19–21]. Moreover, the non-linear characteristics are challenging to solve due to the exponential functions in the characteristic equations. These challenges render determining accurate PV models a puzzle.

Extracting proper parameters of PV models is a thorny issue, and it is primarily solved by three types of methods: point-specific-based methods, traditional numerical optimization methods, and metaheuristic methods [19]. The first category, also referred to as analytical methods, relies heavily on the analytical treatment of the models to reduce the parameters and on specific points to deduce the model parameters [13,22,23]. They generally have low accuracy, especially when there is noise on specific data points. The second category is also known as the deterministic methods, which extensively use the idea of gradients. They are highly exploitable and computationally fast but are sensitive to initialization settings, and the accuracy of the solutions can be insufficient [24–26]. That dilemma is because the PV model's mathematical formulation is implicit, has exponential functions, and requires extraction of multiple parameters. As a result, the mentioned issue has multi-peaked, non-linear, and strongly coupled characteristics, which pose a significant challenge to solving the issue using deterministic methods. Unlike the above two categories, natural phenomena inspire the third class of methods: metaheuristics. They do not rely on gradients and detailed data, are conceptually simple and computationally convenient, and can solve complex optimization issues with high accuracy [27–31]. Therefore, scholars have identified the merits of metaheuristics and applied them to many problems.

Nowadays, the metaheuristics for this paper's problems have evolved considerably, and it is necessary to review the current developments in parameter extraction techniques. Recently, several reviews have partially covered the application of metaheuristics in this area. Abbassi et al. [19] comprehensively described and summarized different indicators and cases and briefly assessed the results. However, the authors were biased towards a broad overview of different methods and ignored details about the metaheuristics' application mechanisms. They merely measured the indicators' presence, without specific results to give the methods' effectiveness. Oliva et al. [32] undertook a dedicated review, tabulated each indicator's results, and described the details of some metaheuristics. Nevertheless, the work mainly focused on PV cells, with insufficient attention to PV modules, and ignored a review of the TDM and algorithmic settings. Venkateswari et al. [33] summarized the indicators and case names, described improved concepts, and compared some metaheuristics. However, they just summarized the minimum root mean square error (RMSE) results and lacked data on other indicators. Li et al. [20] overviewed the environmental factors' presence and surveyed the results of various approaches. However, the review mainly focused on the SDM and DDM and lacked the algorithmic settings of metaheuristics. Overall, the available reviews mainly highlighted the statistics of the RMSE values for SDM and DDM. Specific data on other indicators, i.e., the total number of fitness evaluations (TNFES), the sum of individual absolute errors (SIAE), and the mean, maximum, and standard deviation (STD) of RMSE, were unavailable for judging different methods' performance in computational resources, accuracy, reliability, and robustness. We also note the following shortcomings in past reviews: (a) a lack of holistic evaluation of metaheuristics in recent years for cells and modules, (b) no discussion or literature screening of the situation when the temperature changes, and (c) omission of a presentation of data changes when partial shade is applied.

A holistic view of this type of research takes time to establish for researchers unfamiliar with this area. Meanwhile, the available reviews should include the results of the last several years of study. However, although some reviews comprehensively summarize all solutions to the problem, they mention too few metaheuristics and need more numerical details. Others focus on PV cells and modules, but omit the analysis of metaheuristics. These shortcomings make their conclusions rather one-sided and make it difficult for the reader to understand the research results from multiple dimensions. Therefore, a persuasive article that considers the model's various aspects, the parameter settings, and the evaluation metrics and integrates the results of a large number of applications of metaheuristics to the problem is needed to present the recent research results. This paper provides a comprehensive and detailed summary and analysis of the application of metaheuristics to model PV accurately in recent years. Specifically, the metaheuristics are categorized and their rationale is outlined. The algorithmic settings are summarized, and the results are compared and ranked in various indicators. The variation of the parameters in different environments is studied, and a brief description of the relevant literature in recent years is given. Some cell models that are temporarily not in widespread use today but are of high research value are analyzed. Then, their advantages and disadvantages are analyzed, and the remaining challenges are analyzed. Eventually, future directions for research are summarized in solution approaches and application scenarios.

This work's main contributions are as follows:

- The mathematical models of current commonly used SDM, DDM, TDM, and PV modules are explained;
- The characteristics of each metaheuristic method and their enhancements and applications are outlined;
- The statistical results of RMSE, TNFES, SIAE and algorithmic settings of selected metaheuristics are summarized and compared;
- The output characteristics of the PV system are discussed for the dynamic temperature, irradiance, and partial shading, and the variation in parameters and RMSE are analyzed;
- Existing challenges and possible future work focuses are analyzed and provided.

The remainder is briefly sketched as follows. The PV cell's mathematical model and the evaluation indicators are explained in Section 2. Section 3 illustrates different metaheuristics. Section 4 provides an overall analysis of different methods, existing challenges, and possible research directions. Finally, Section 5 gives the conclusion.

2. PV Models and Problem Formulations

Several PV models and their corresponding equivalent circuits are revealed in the first part of this section, to quantify the electrical characteristics of PV systems. Directly comparing PV models' parameters extracted by different methods is not easy. To objectively appraise the extracted results of different methods, the second part of this section gives several indicators commonly used to evaluate the experimental results.

2.1. PV Models

SDM, DDM, and TDM models have been widely used by researchers in recent years [20]. In general, more diodes in a circuit represent a more accurate model, but also increase the model complexity [33].

2.1.1. SDM

Figure 1a mentions the equivalent schematic of the SDM. The output voltage and current are V and I, respectively, and the electrical expression of I is shown below [34,35].

$$I = I_{ph} - I_{sh} - I_{sd} = I_{ph} - \frac{V + IR_s}{R_{sh}} - I_{ssd}\left[\exp\left(\frac{q(V + IR_s)}{nkT}\right) - 1\right] \tag{1}$$

where I_{ph}, I_{sh}, I_{sd}, and I_{ssd} represent the photogenerated line current, shunt resistor line current, diode line current, and diode saturation current, respectively. R_s and R_{sh} represent the series resistance and branch resistance, respectively. n represents the ideal factor. T, k, and q represent the Boltzmann constant (1.3806×10^{-23} J/K), absolute temperature, and unit charge (1.6022×10^{-19} C).

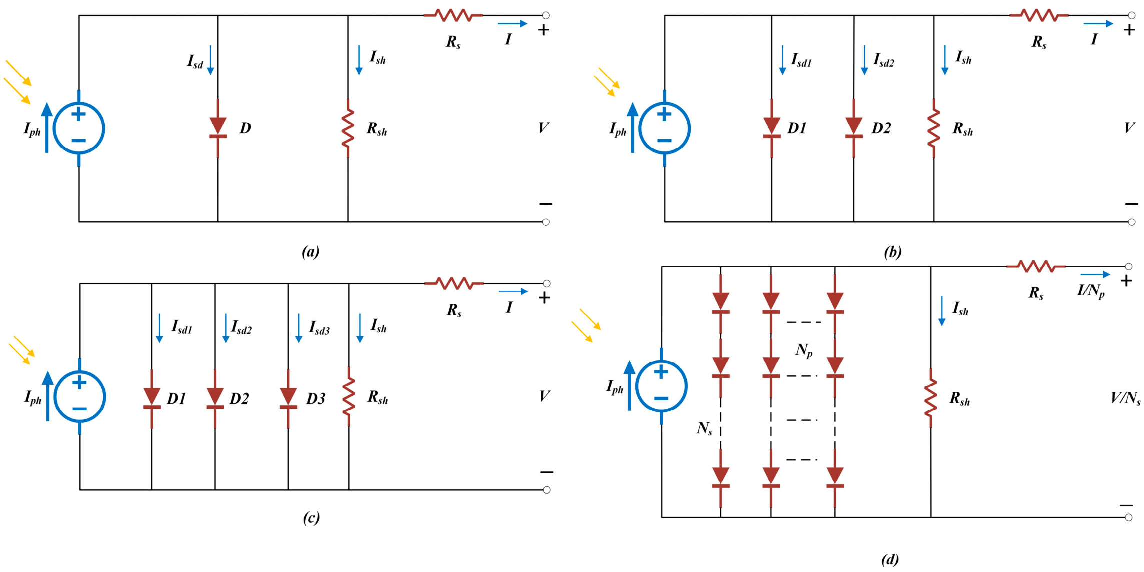

Figure 1. PV models' circuits: (**a**) SDM; (**b**) DDM; (**c**) TDM; (**d**) PV module.

The above demonstrates that accurate modeling requires estimating the values of I_{ph}, I_{ssd}, n, R_s, and R_{sh}.

2.1.2. DDM

Figure 1b mentions the equivalent schematic of the DDM. After adding a diode, below is the electrical expression of I [36,37].

$$I = I_{ph} - I_{sh} - I_{sd1} - I_{sd2} = I_{ph} - \frac{V + IR_s}{R_{sh}} - I_{ssd1}\left[\exp\left(\frac{q(V + IR_s)}{n_1 kT}\right) - 1\right] - I_{ssd2}\left[\exp\left(\frac{q(V + IR_s)}{n_2 kT}\right) - 1\right] \quad (2)$$

where I_{sd1} and I_{sd2} represent the first and second diode line currents, respectively, I_{ssd1} and I_{ssd2} represent the corresponding diode saturation currents, and n_1 and n_2 represent the corresponding ideal factors.

This model needs to estimate the values of I_{ph}, I_{ssd1}, I_{ssd2}, n_1, n_2, R_s, and R_{sh}.

2.1.3. TDM

Figure 1c mentions the equivalent schematic of the TDM. Below is the electrical expression of I [38–40].

$$I = I_{ph} - I_{sh} - \sum_{j=1 \to 3} I_{sdj} = I_{ph} - \frac{V + IR_s}{R_{sh}} - \sum_{j=1 \to 3} I_{ssdj}\left[\exp\left(\frac{q(V + IR_s)}{n_j kT}\right) - 1\right] \quad (3)$$

where I_{sdj}, I_{ssdj}, and n_j represent the jth diode line current, the saturation current, and the ideal factor, respectively.

The TDM requires estimating the values of I_{ph}, I_{ssd1}, I_{ssd2}, I_{ssd3}, n_1, n_2, n_3, R_s, and R_{sh}.

2.1.4. PV Module

Figure 1d mentions the equivalent schematic of the PV module based on the SDM. A PV module composed of $N_s \times N_p$ cells inherently has a high complexity. Therefore, using the SDM to construct PV modules is the first choice for most researchers. Equation (4) is the electrical expression of the PV module's current [4,41].

$$I = I_{ph}N_p - \frac{V + IR_sN_s/N_p}{R_{sh}N_s/N_p} - I_{ssd}N_p\left[\exp\left(\frac{q(V + IR_sN_s/N_p)}{nN_skT}\right) - 1\right] \quad (4)$$

The PV module has the same parameters as the SDM (I_{ph}, I_{ssd}, n, R_s, and R_{sh}).

2.1.5. PV Model Review

Although the SDM, with its simple structure and fair accuracy, is presented at the very beginning of this section, it is not the earliest cell model. It is a development of the ideal PV cell model (IPCM). Compared to the IPCM, which has a straightforward structure consisting of only a current source and diode, the SDM simulates the flow resistance, electrode resistance, and surface contact resistance, explains the physical behavior, and is widely used in this problem [42]. To further improve the accuracy of the model's simulated conduct at low irradiance, a diode is added to the DDM to represent the loss of current in the depletion region. However, the added unknown parameters increase the difficulty of the solution. TDM has the potential to achieve higher accuracy than DDM after calculating the leakage current and grain boundaries with the addition of a diode. Again, the solution difficulty increases as the dimensionality of the problem increase.

In addition, there are many less commonly used improved diode models, such as the modified 3-diode model [43], the SDM with capacitance [44], the Generalized Multi-Dimension Diode Model [45], the Modified SDM (MSDM) [46], the Four Diode Model (FDM) [47], the Modified DDM (MDDM) [48] and the Modified TDM (MTDM) [49]. We note that metaheuristics have recently been used to solve the FDM and the modified SDM, DDM, and TDM models. Thus, it would be a trend for future research to consider these four models to find a cell model that matches the proposed method to achieve a balance between solution difficulty and accuracy.

For the modules, in addition to the SDM presented in Section 2.1.4, the use of DDM and TDM formations are also options considered by the researchers. Their accuracy and solution difficulty performance are similar to their performance in the cell model. The appropriate model-building module must be selected to fit the specific needs. In this paper, considering that counting all the above models would cause duplication of content, excessive length, and difficulty reading, only the computational results of the modules composed of SDM components are summarized. The increased accuracy, increased difficulty in solving, and increased computational resources due to the increase in diodes will be reflected in the computational results of the cell model.

In addition, several specific PV models exist to achieve accurate modeling of PV systems in specific situations. They are not commonly used for the time being, but are of great interest. The dynamic PV model is one of them. It considers underdamped currents, switching frequency harmonics, varying loads, and resonance of cables, and is more suitable for grid-connected operation [50,51]. Its equivalent circuit diagram is shown in Figure 2 [52].

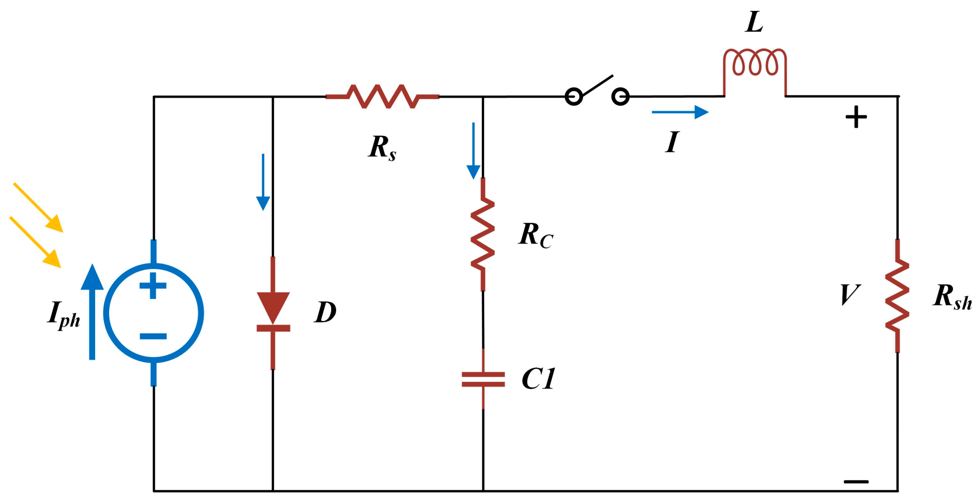

Figure 2. Dynamic model's circuits.

The model's output current is shown as follows [53]:

$$\begin{cases} I(s) = \frac{a_{21}(s+b_1)+b_2(s-a_{11})}{(s-a_{11})(s-a_{22})-a_{21}a_{12}} \cdot \frac{V_{OC}}{s} \\ \begin{pmatrix} a_{11} & a_{12} \\ a_{21} & a_{22} \end{pmatrix} = \begin{pmatrix} \frac{-1}{C(R_s+R_C)} & \frac{-R_s}{C(R_s+R_C)} \\ \frac{R_s}{L(R_s+R_C)} & \frac{-(R_C R_L+R_C R_s+R_L R_s)}{L(R_s+R_C)} \end{pmatrix}, \begin{pmatrix} b_1 \\ b_2 \end{pmatrix} = \begin{pmatrix} \frac{1}{C(R_s+R_C)} \\ \frac{R_C}{L(R_s+R_C)} \end{pmatrix} \end{cases} \tag{5}$$

where s is the time, R_s and the open circuit voltage V_{oc} are usually known, the inductor L, the resistor R_C, and the capacitor C are unknown. Therefore, C, R_C, and L are the parameters to be extracted.

2.2. Problem Formulations

RMSE between the measured data and the calculated data usually serves as the objective function [54–56]:

$$\text{RMSE} = \sqrt{\frac{1}{N}\sum_{k=1}^{N} f^2(V, I, x)} \tag{6}$$

where x represents the solution vector and N represents the actual data's amount, and $f(V, I, x)$ calculates the current error in the following way.

For SDM:

$$\begin{cases} f(V, I, x) = I_{ph} - \frac{V+IR_s}{R_{sh}} - I_{ssd}\left[exp\left(\frac{q(V+IR_s)}{nkT}\right) - 1\right] - I \\ x = \left(I_{ph}, I_{ssd}, R_s, R_{sh}, n\right) \end{cases} \tag{7}$$

For DDM:

$$\begin{cases} f(V, I, x) = I_{ph} - \frac{V+IR_s}{R_{sh}} - I_{ssd1}\left[\exp\left(\frac{q(V+IR_s)}{n_1 kT}\right) - 1\right] - I_{ssd2}\left[\exp\left(\frac{q(V+IR_s)}{n_2 kT}\right) - 1\right] - I \\ x = (I_{PV}, I_{ssd1}, I_{ssd2}, R_s, I_{sh}, n_1, n_2) \end{cases} \tag{8}$$

For TDM:

$$\begin{cases} f(V, I, x) = I_{ph} - \frac{V+IR_s}{R_{sh}} - \sum\limits_{j\to 3} I_{ssdj}\left[\exp\left(\frac{q(V+IR_s)}{n_j kT}\right) - 1\right] - I \\ x = (I_{PV}, I_{ssd1}, I_{ssd2}, I_{ssd3}, R_s, I_{sh}, n_1, n_2, n_3) \end{cases} \tag{9}$$

For PV module:

$$\begin{cases} f(V, I, x) = I_{ph}N_p - \frac{V+IR_s N_s/N_p}{R_{sh}N_s/N_p} - I_{ssd}N_p\left[\exp\left(\frac{q\left(V+IR_s N_s/N_p\right)}{nN_s kT}\right) - 1\right] - I \\ x = \left(I_{ph}, I_{ssd}, R_s, R_{sh}, n\right) \end{cases} \tag{10}$$

For the objective function RMSE, its computation requires solving methods with the ability to solve implicit functions. Commonly used are deterministic and metaheuristic methods. Several deterministic methods, including Newton Raphson [24], Lambert W function [25], Levenberg Marquardt [57], and Berndt–Hall–Hall–Hausman [58], have successfully solved the non-linear problem. However, it does not mean that deterministic methods can tackle the challenge of initial value sensitivity well. Due to challenges such as non-linearity and non-convexity, metaheuristics are considered to be the best solution for solving this issue.

2.3. Indicators Summary

Varied algorithmic settings substantially affect the results of metaheuristic methods and various indicators can evaluate the results from diverse aspects. Hence, we summarize the approach and case settings and the performance evaluation indicators. Usually, the literature has drawn characteristic curves to visualize the accuracy of the extracted parameters. Nevertheless, when the parameters' difference is not very large, some general and objective indicators are used as the basis for evaluating the advantages and disadvantages of different methods. Here, we highlight the commonly used indicators to compare them:

- Individual absolute error (IAE): it represents the difference between the actual and simulated current values [28,30];
- Sum of IAEs (SIAE) and mean IAEs (MIAE): they are more holistic in evaluating the accuracy of the simulated data [29,59];
- RMSE: it focuses on overall assessment of the data's dispersion [31,60];
- Friedman test (FT), Wilcoxon rank sum test (WRT), and Wilcoxon signed rank test (WST): they broaden evaluation scales from statistical perspectives;

$$\mathrm{IAE} = |f(V, I, x)| \tag{11}$$

$$\mathrm{SIAE} = \sum_{k=1}^{N} IAE \tag{12}$$

$$\mathrm{MIAE} = \frac{1}{N}\sum_{k=1}^{N} IAE \tag{13}$$

- In addition, a few works in the literature also use evaluation indicators such as the sum of squares of power, current, and voltage errors (ERR) [61].

3. Methods and Results

Metaheuristics have no special data or environment requirements and have high robustness and accuracy in this studied issue, which is also the reason that they have been frequently used. Different metaheuristics were inspired by various things when they were developed. Figure 3 categorizes the metaheuristics into four genres by the type each one simulates, i.e., evolution-based methods (GA, DE, JAYA), human social activity-based methods (GSK, SDO, TLBO), animal activity-based methods (PSO, ABC, GWO, WOA, HHO), and natural phenomenon-based methods (TGA, SOS, FPOA). In this section, the widely used metaheuristics for solving this issue, namely GA, DE, PSO, ABC, GWO, JAYA, TLBO, and WOA, are selected and briefly described. They share a high degree of similarity in the optimization process. For brevity, Figure 4 gives the general flowchart of metaheuristics.

3.1. GAs

The survival of the fittest phenomenon inspires the evolutionary algorithm, i.e., genetic algorithm. A solution is encoded as binary chromosomes, and all chromosomes are updated through iteration and fitness assessment. Selection, crossover, and mutation are the iteration's three primary operations. The first operation is related to the fitness value and usually uses roulette, random traversal sampling, and ranked selection. The second operation improves exploitation by changing the subsequence of random loci between chromosomes, and the third operation improves exploration by changing genes on individual chromosomes [62].

In [63], the authors used GA in 30XLS and 34XLS PV modules. Characteristic curves were plotted to visualize the accuracy. However, the method of validating the results was relatively simple. In [64], an adaptive genetic algorithm (AGA) was designed, employing the Pearson residual reduction and minimum mean square error reduction techniques. Relevant manufacturer data at different temperatures verified the AGA's accuracy. However, it lacked the comparison under different light intensities, and the validation was too homogeneous. For intelligent algorithms, more data-based optimization often means more accurate results. Therefore, Harrag et al. [65] combined genetic algorithms with neural networks and proposed a metaheuristic based on genetic neural networks (GNN). GNN's effectiveness was verified on the SDM and DDM with the *RMSE*.

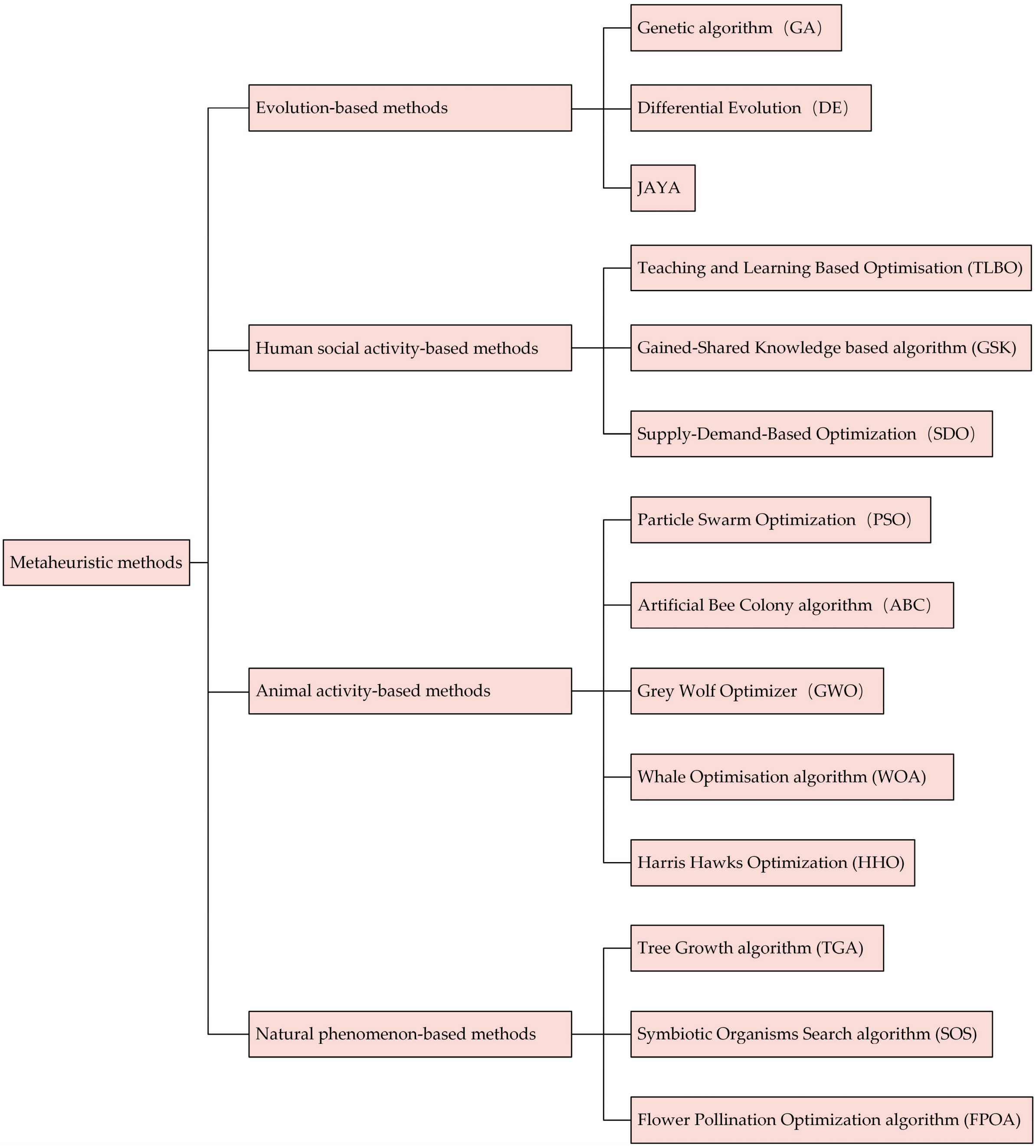

Figure 3. Metaheuristic methods' genres.

Table 1 lists essential information on GA variants. Among them, the squared error for GA was 5.8297×10^{-8} and 3.0751×10^{-7}, which is highly accurate, but there is a lack of comparison algorithms to judge the competitiveness of this result. AGA did not give any numerical RMSE values. The minimum *RMSE* for GNN reached the order of 1×10^{-3}, yet almost all recent state-of-the-art algorithms reached the order of 1×10^{-4}. The GA variants' performance is not ranked in this section, as the current GA variants did not use the same metric function.

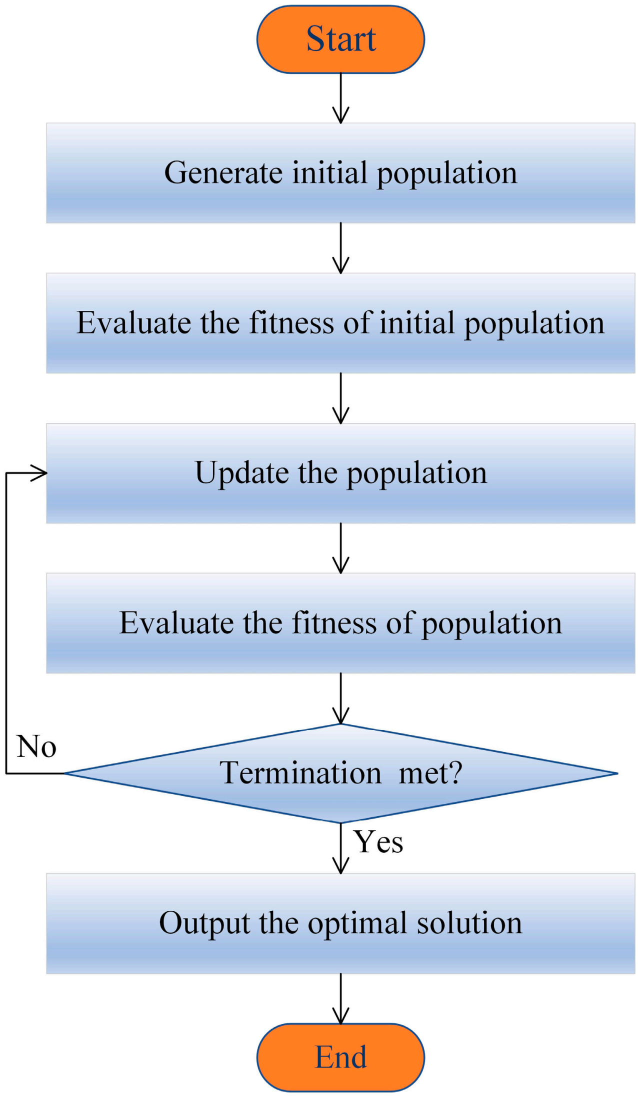

Figure 4. Metaheuristics' general flowchart.

Table 1. GAs' essential information and metrics.

Method	Main Contributors	Case	Algorithmic Parameter	Indicator	TNFES	Run
GA [63]	Harrag et al., CCNS Laboratory, Department of Electronics, Faculty of Technology, Ferhat Abbas University	30XLS 34XLS	NP = 100, CP = 0.5, MP = 0.02	SE	10,000	-
AGA [64]	Kumari et al., School of Electrical Engineering, VIT University	-	C1 = 0.01, C2 = 0.001	-	-	-
GNN [65]	Wang et al., Zhengzhou University of Aeronautics	SDM DDM	NP = 30 NP = 50	RMSE RMSE	9000 15,000	80 80

3.2. DEs

DE is fast in converging, simple in structure, and easy to implement [66,67]. As a population-based metaheuristic, DE has the same three operations with GA. DE individuals achieve mutation by adding different weight coefficients to the product of the difference between two individuals. The crossover is used to produce a trial vector from the target individual and the mutant vector. The selection usually chooses a greedy selection scheme to retain fitter individuals.

In [68], an improved adaptive DE (IADE) with exponential scaling factor (F) and crossover rate (CR) based on automatic performance updates was presented. The results' accuracy was verified using PV data with different temperatures and light intensities in terms of mean RMSE and fitted plots. Biswas et al. [61] designed a novel successful history-based DE (L-SHADE) with a linear reduced population size (NP) technique. Its parameter estimation was implemented using three particular points. The results showed that the error was almost zero. In [23], Chin et al. designed a differential evolution based on three points to improve the speed and accuracy of L-SHADE. In [69], an enhanced adaptive differential evolution (EJADE) was implemented by cross-ranking and dynamic population reduction techniques, and the algorithm's reliability was verified well. Xiong et al. [70] designed a new method (QILDE) for developing optimal value fields by adding quadratic interpolation to the crossover step. Applications of QILDE to six different PV models showed its strong competitiveness in different cases. In [71], a new method (EBLSHADE) based on SHADE with the linear population size reduction technique and greedy variation technique was designed. Its practical application in PV models demonstrated its importance in optimizing PV model parameters. In [72], dynamic control factors, including mutation and crossover, were designed and introduced into DE to form the new method called DEDCF. In [73], the authors designed a directed permutation differential evolution (DPDE) using the information on the direction of movement of populations and individuals, and applied it to a solar cell model. Hu et al. [41] designed a novel DE (RLDE) with reinforcement learning that adjusts the value of F by the Q-learning to achieve automatic parameter tuning, and compared RLDE with other methods, showing its superior robustness and accuracy. A heterogeneous differential evolution (HDE) was built in [74] with two improved mutation methods, a heterogeneous technique and an information exchange technique. It was demonstrated that the performance of HDE was representative in multiple dimensions through its application to the problems covered in this study. Kharchouf et al. [75] introduced Lambert's W function and metaheuristic techniques to DE for preferential F and CR, and named the method MSDE. It demonstrated high success through application. In [76], a novel DE (FADE) capable of optimizing F and CR was designed by employing fuzzy selection techniques and adaptive parameter tuning techniques. SIAE and RMSE demonstrated its excellent accuracy and robustness.

Tables 2 and 3 show the essential information and numerical metrics for each DE's variant, respectively. It is noticeable that there are many recent studies on DE, and most of them have obtained excellent performance. Regarding resource consumption, DE3P has the least, at 2500, followed by EBLSHADE, DEDCF, MSDE, EJADE, QILDE, RLDE, L-SHADE, DPDE, HDE, FADE, and IADE, respectively. Since ERRs were rarely used, data for WRT, WST, FT, and IAE were unavailable for statistics, and SIAE and MIAE are similar, we tabulate specific data for SIAE and various types of RMSE in Table 3 for comparison. To achieve a comprehensive accuracy comparison across multiple cases, the SDM, DDM, and Photowatt-PWP201 with the minimum RMSE values are used for the combined ranking. According to the FT results, MSDE (1.333) ranks first, followed by DEDCF (1.667), EJADE (4.333), QILDE (4.333), RLDE (4.333), HDE (4.667), DPDE (5.333), and EBLSHADE (5.833). However, EBLSHADE achieves excellent accuracy even though it is in last place, so future research in DE could further focus on reducing resource consumption and achieving improved performance in multiple accuracy evaluation metrics.

3.3. PSOs

PSO is a hot topic in artificial intelligence. The particle's new position is a combination of the current position and the updated velocity. The updating of the velocity is composed of three parts, and the first part is the current velocity scaled by the weight factor (w). The second part is the individual best position to steer the current position under the weight of the learning factor (c_1) and a random variable ($r1$). The third part is the global best position to steer the current position under the weight of the learning factor (c_2) and a random variable ($r2$). The $r1$ and $r2$ are unrelated, as are the c_1 and c_2 [77,78].

Table 2. DEs' essential information and metrics.

Method	Main Contributors	Case	Algorithmic Parameter	Indicator	TNFES	Run
IADE [68]	Jiang et al., School of Computer Engineering, Nanyang Technological University	SDM Photowatt-PWP201 SL80CE-36M	Iteration = 8000, $a = \ln 2$, $b = 0.5$	RMSE	-	30 30 -
L-SHADE [61]	Biswas et al., School of Electrical and Electronic Engineering, Nanyang Technological University	Kyocera KC200GT Shell SQ85 Shell ST40	$NP = 50$, $F = rand\ (0.1, 0.5)$, $CR = rand\ (0.1, 0.5)$	ERR	50,000	30
DE3P [23]	Chin et al., Centre of Electrical Energy Systems, School of Electrical Engineering, Universiti Teknologi Malaysia	SDM Photowatt-PWP201 STM6-40/36 STP6-120/36	$NP = 50$, $F = 0.7$, $CR = 0.8$	RMSE SIAE MIAE	2500	35
EJADE [69]	Li et al., School of Computer Engineering, Hubei University of Arts and Science	SDM DDM Photowatt-PWP201 STM6-40/36 STP6-120/36	$NP_{max} = 50$, $NP_{min} = 4$	RMSE	10,000 20,000 10,000 15,000 15,000	30
QILDE [70]	Xiong et al., Guizhou Key Laboratory of Intelligent Technology in Power System, College of Electrical Engineering, Guizhou University	SDM DDM Photowatt-PWP201 STM6-40/36 STP6-120/36 Sharp ND-R250A5	$F = rand\ (0.1, 1)$, $CR = rand\ (0, 1)$	RMSE FT	10,000 20,000 10,000 30,000 30,000 30,000	50 50 50 50 50 50
EBLSHADE [71]	Song et al., School of Computer Science and Technology, Shandong Technology and Business University	SDM DDM Photowatt-PWP201 STM6-40/36 STP6-120/36	$NP = 50$, $H = 100$, $w1 = 0.2$, $w2 = 0.6$, $pmin = 0.05$, $pmax = 0.2$	RMSE IAE	4000 10,000 5000 10,000 15,000	30 30 30 30 30
DEDCF [72]	Parida et al., Department of Electrical Engineering, ITER, Siksha O Anusandhan	SDM DDM Photowatt-PWP201	$NP = 10D$, $F = rand\ (0.1, 0.9)$, $CR = rand\ (0, 1)$	RMSE MIAE	10,000 14,000 10,000	50 50 50
DPDE [73]	Gao et al., Faculty of Engineering, University of Toyama	SDM DDM TDM Photowatt-PWP201 STM6-40/36 STP6-120/36	$NP = 18D$, $H = 5$, $p = 0.11$	RMSE SIAE WRT FT	50,000	30
RLDE [41]	Hu et al., School of Computer Science, China University of Geosciences	SDM DDM Photowatt-PWP201 STM6-40/36 STP6-120/36	$NP = 30$, $f = -0.1$ or 0 or 0.1, $CR = 0.9$	RMSE	30,000	30
HDE [74]	Wang et al., School of Software, Yunnan University	SDM DDM TDM Photowatt-PWP201 STM6-40/36 STP6-120/36	$NP = 30$, $p = 0.1$	RMSE WRT FT	50,000	30
MSDE [75]	Kharchouf et al., University Abdelmalek Essadi, FSTT	SDM DDM Photowatt-PWP201 STM6-40/36	$NP = 10D$, $F = 0.7$, $CR = 0.8$	RMSE	10,000 14,000 10,000 10,000	30
FADE [76]	Dang et al., Institute for Electrical Power and Integrated Energy of Shaanxi Province, Xi'an University of Technology	Photowatt-PWP201 STM6-40/36 STP6-120/36	$NP = 25$, $uF^{init} = 0.7$, $CR^{init} = 0.5$	RMSE SIAE	75,000	30

Ben et al. [79] applied PSO to the SDM and compared it with other methods, concluding that PSO outperformed other methods with data supporting. In [80], Ni et al. presented an adaptive elite mutation technique for PSO (PSO-AEM) for a domain search of the optimal global position of PSO, and found that PSO-AEM had a faster speed and higher accuracy. Merchaoui et al. [81] found that PSO was prone to premature convergence, so an adaptive mutation technique was proposed and introduced into PSO to form an improved MPSO. MPSO achieved good IAE and RMSE values and fitted the characteristic curves well at different temperatures and light intensities. In [82], Guaranteed Convergent Particle Swarm Optimization (GCPSO) was presented to avoid premature convergence. In [83], an enhanced leader PSO (ELPSO) using five mutation operators to enhance the leader was designed, following the idea that a high-quality leader could pull the solution towards the excellent region. The identification results showed that ELPSO effectively improved the quality of PSO solutions. In [84], the authors presented an improved PSO (SAIW-PSO) which used the simulated annealing technique to control w and introduced a deterministic method for optimizing the current values. The fitting results supported the view that SAIW-PSO was accurate, fast, and effective. Kiani et al. [85] designed a dynamic inertia weight PSO (DEDIWPSO) with a double exponential function to mitigate the premature convergence. This method demonstrated excellent validity, reliability, and accuracy in the issue covered in this work. The authors in [86] implemented PSO in parallel (PPSO) on a modern graphics processing unit (GPU). They demonstrated the very high accuracy and short elapsed time of PPSO by estimating multiple PV models' parameters. In [87], an enhanced PSO (PSO-ST) was developed using sinusoidal chaos and tangential chaos techniques to adjust the weight and learning factors. Inspired by cuckoo search random reselect parasitic nests, Fan et al. [88] developed a new method (PSOCS) by combining the random reselection strategy with PSO. The application results showed PSOCS's stability and effectiveness.

Table 3. DEs' experiment results.

Method	Case	SIAE	MIN RMSE	Mean RMSE	MAX RMSE	STD of RMSE	Rank
IADE [68]	SDM	-	9.8900×10^{-4}	-	-	-	N/A
	Photowatt-PWP201	-	2.4000×10^{-3}	-	-	-	
	SL80CE-36M	-	1.15×10^{-2}	-	-	-	
DE3P [23]	SDM	0.0172	8.1291×10^{-4}	-	-	-	N/A
	Photowatt-PWP201	0.0505	2.422747×10^{-3}	-	-	-	
	STM6-40/36	0.0210	1.774×10^{-3}	-	-	-	
	STP6-120/36	0.2091	1.4091×10^{-2}	-	-	-	
EJADE [69]	SDM	-	9.8602×10^{-4}	9.8602×10^{-4}	9.8602×10^{-4}	5.13×10^{-17}	4.333
	DDM	-	9.8248×10^{-4}	9.8363×10^{-4}	9.8602×10^{-4}	1.36×10^{-6}	
	Photowatt-PWP201	-	2.4251×10^{-3}	2.4251×10^{-3}	2.4251×10^{-3}	3.27×10^{-17}	
	STM6-40/36	-	1.7298×10^{-3}	1.7298×10^{-3}	1.7298×10^{-3}	5.94×10^{-18}	
	STP6-120/36	-	1.6601×10^{-2}	1.6601×10^{-2}	1.6601×10^{-2}	2.33×10^{-17}	
QILDE [70]	SDM	0.01770381	9.8602×10^{-4}	9.8603×10^{-4}	9.8616×10^{-4}	2.7839×10^{-8}	4.333
	DDM	0.01731807	9.8248×10^{-4}	9.8480×10^{-4}	9.8968×10^{-4}	1.5868×10^{-6}	
	Photowatt-PWP201	0.04178701	2.4251×10^{-3}	2.4257×10^{-3}	2.4370×10^{-3}	2.2436×10^{-6}	
	STM6-40/36	0.02177419	1.7298×10^{-3}	1.7298×10^{-3}	1.7298×10^{-3}	1.1295×10^{-17}	
	STP6-120/36	0.27797426	1.6601×10^{-2}	1.6601×10^{-2}	1.6601×10^{-2}	2.8518×10^{-14}	
	Sharp ND-R250A5	0.21759981	1.1183×10^{-2}	1.1183×10^{-2}	1.1183×10^{-2}	5.1647×10^{-10}	
EBLSHADE [71]	SDM	-	9.8602×10^{-4}	9.8602×10^{-4}	-	1.9169×10^{-15}	5.833
	DDM	-	9.8295×10^{-4}	9.8574×10^{-4}	-	1.2825×10^{-6}	
	Photowatt-PWP201	-	2.4251×10^{-3}	2.4251×10^{-3}	-	2.8821×10^{-17}	
	STM6-40/36	-	1.7298×10^{-3}	1.7298×10^{-3}	-	6.40591×10^{-14}	
	STP6-120/36	-	1.6601×10^{-2}	1.6601×10^{-2}	-	8.0544×10^{-16}	
DEDCF [72]	SDM	-	7.730062×10^{-4}	-	-	-	2
	DDM	-	7.419648×10^{-4}	-	-	-	
	Photowatt-PWP201	-	2.05296×10^{-3}	-	-	-	
DPDE [73]	SDM	0.02153	$9.86021877891470 \times 10^{-4}$	$9.86021877891542 \times 10^{-4}$	$9.86021877891588 \times 10^{-4}$	$2.57114481592195 \times 10^{-17}$	5.333
	DDM	0.021276	$9.82484827161920 \times 10^{-4}$	$9.82549779378988 \times 10^{-4}$	$9.83081420487992 \times 10^{-4}$	$1.51333797156833 \times 10^{-7}$	
	TDM	0.021275	$9.82484851785319 \times 10^{-4}$	$9.83096769943567 \times 10^{-4}$	$9.86188097663681 \times 10^{-4}$	$1.02284590208062 \times 10^{-6}$	
	Photowatt-PWP201	0.048924	$2.42507486809506 \times 10^{-3}$	$2.42507486809511 \times 10^{-3}$	$2.42507486809514 \times 10^{-3}$	$1.82238517018742 \times 10^{-17}$	
	STM6-40/36	0.021903	$1.72981370994065 \times 10^{-3}$	$1.72981370994068 \times 10^{-3}$	$1.72981370994070 \times 10^{-3}$	$1.09732017119964 \times 10^{-17}$	
	STP6-120/36	0.317128	$1.66006031250851 \times 10^{-2}$	$1.66006031250854 \times 10^{-2}$	$1.66006031250855 \times 10^{-2}$	$7.66886076234863 \times 10^{-17}$	
RLDE [41]	SDM	-	9.8602×10^{-4}	9.8602×10^{-4}	9.8602×10^{-4}	3.4834×10^{-17}	4.333
	DDM	-	9.8248×10^{-4}	9.8695×10^{-4}	9.8457×10^{-4}	1.7498×10^{-6}	
	Photowatt-PWP201	-	2.4251×10^{-3}	2.4251×10^{-3}	2.4251×10^{-3}	6.3084×10^{-17}	
	STM6-40/36	-	1.7298×10^{-3}	1.7298×10^{-3}	1.7298×10^{-3}	1.5784×10^{-17}	
	STP6-120/36	-	1.6601×10^{-2}	1.6601×10^{-2}	1.6601×10^{-2}	1.9764×10^{-16}	
HDE [74]	SDM	0.021527	$9.86021877891313 \times 10^{-4}$	$9.86021877891456 \times 10^{-4}$	$9.86021877891534 \times 10^{-4}$	$4.56994495305984 \times 10^{-17}$	4.667
	DDM	0.021275	$9.82484851785123 \times 10^{-4}$	$9.84154478759700 \times 10^{-4}$	$9.86021877891565 \times 10^{-4}$	$1.67264373173134 \times 10^{-6}$	
	TDM	0.021275	$9.82484851785213 \times 10^{-4}$	$9.82852008467139 \times 10^{-4}$	$9.88358683960422 \times 10^{-4}$	$1.08111146060101 \times 10^{-6}$	
	Photowatt-PWP201	0.048924	$2.42507486809496 \times 10^{-4}$	$2.42507486809504 \times 10^{-4}$	$2.42507486809510 \times 10^{-3}$	$3.15406568173825 \times 10^{-17}$	
	STM6-40/36	0.021903	$1.72981370994065 \times 10^{-3}$	$1.72981370994068 \times 10^{-3}$	$1.72981370994070 \times 10^{-3}$	$7.89430228096153 \times 10^{-18}$	
	STP6-120/36	0.31713	$1.66006031250847 \times 10^{-2}$	$1.66006031250851 \times 10^{-2}$	$1.66006031250855 \times 10^{-2}$	$1.86128634500124 \times 10^{-16}$	
MSDE [75]	SDM	-	7.7692×10^{-4}	-	-	-	1.333
	DDM	-	7.63×10^{-4}	-	-	-	
	Photowatt-PWP201	-	1.7298×10^{-3}	-	-	-	
	STM6-40/36	-	2.0529×10^{-3}	-	-	-	
FADE [76]	Photowatt-PWP201	0.0489237	2.42507×10^{-3}	2.42507×10^{-3}	2.42507×10^{-3}	-	N/A
	STM6-40/36	0.0219033	1.72981×10^{-3}	1.72981×10^{-3}	1.72981×10^{-3}	-	
	STP6-120/36	0.3171278	1.66006×10^{-2}	1.66006×10^{-2}	1.66006×10^{-2}	-	

The "N/A" means that there is insufficient data to support an average algorithm ranking using the Friedman Test on the three cases: SDM, DDM, and Photowatt-PWP201.

Tables 4 and 5 combine the essential information and numerical metrics of the PSO's variants. In the past five years, there have been numerous studies on PSO. Regarding resource consumption, PSO-AEM has the lowest TNFES of 10,000, followed by PSOCS, PSO, ELPSO, MPSO, SAIW-PSO, DEDIWPSO, PSO-ST, GCPSO, and PPSO. Regarding the ranking of MIN RMSE metrics, DEDIWPSO is first, followed by PSO-ST, GCPSO, MPSO, PPSO, and PSOCS. Although DEDIWPSO has the highest accuracy, it consumes massive computational resources. Hence, a considerable reduction in computational resource consumption while keeping accuracy constant is worthy of further research.

Table 4. PSOs' essential information and metrics.

Method	Main Contributors	Case	Algorithmic Parameter	Indicator	TNFES	Run
PSO [79]	Ben et al., Laboratory of Electronics, Signal Processing and Physical Modeling, Faculty of Sciences of Agadir Ibn Zohr University	SDM	NP = 50, Iteration = 1000, w = 0.4, $c_1 = c_2 = 2$	RMSE IAE	-	-
PSO-AEM [80]	Ni et al., Institute of Equipment Supervision and Inspection; Suzhou Nuclear Power Research Institute	-	NP = 50	-	10,000	-
MPSO [81]	Merchaoui et al., Electrical Department, National Engineering School of Monastir, University of Monastir	SDM DDM Photowatt-PWP201 IFRI250-60	NP = 60, Iteration = 2000, w = 0.4, $c_1 = c_2 = 2$	RMSE IAE	-	-
GCPSO [82]	Nunes et al., Department of Electromechanical Engineering, University of Beira Interior	SDM DDM Photowatt-PWP201 Sharp ND-R250A5	$NP = 20D$, Iteration = 10,000, w = 0.55, $c_1 = 1$, $c_2 = 2$	RMSE SIAE	-	100
ELPSO [83]	Rezaee et al., Department of Electrical Engineering, Lashtenesha-Zibakenar Branch, Islamic Azad University	SDM DDM STM6-40/36	NP = 991, $c_1 = 1$, $c_2 = 2$ NP = 1489, $c_1 = 1$, $c_2 = 2$ NP = 991, $c_1 = 1$, $c_2 = 2$	RMSE IAE	101,000 151,500 101,000	30
SAIW-PSO [84]	Kiani et al., Department of Electrical Engineering, University of Engineering and Technology, Taxila	SDM DDM	NP = 100, Iteration = 10,000,	RMSE	-	100
DEDIWPSO [85]	Kiani et al., Department of Electrical Engineering, University of Engineering and Technology, Taxila	SDM DDM Photowatt-PWP201 JKM330P-72	NP = 100, Iteration = 10,000, w^{init} = 0.8	RMSE IAE	-	30
PPSO [86]	Gao et al., Department of Electrical and Computer Engineering, National University of Singapore	SDM DDM Photowatt-PWP201	*DDM:* NP = 6400, Others: NP = 3200, w = 0.5, c_1 = 2.5, c_2 = 1.6	RMSE	640,000 2,560,000 640,000	30
PSO-ST [87]	Kiani et al., Department of Electrical Engineering, University of Engineering and Technology, Taxila	SDM DDM Photowatt-PWP201 JKM330P-72	NP = 100, Iteration = 10,000,	RMSE SIAE	-	30
PSOCS [88]	Fan et al., College of Electrical and Electronic Engineering, Wenzhou University	SDM DDM Photowatt-PWP201 SM55 KC200GT ST40	NP = 30	RMSE	20,000	30 -

Table 5. PSOs' experiment results.

Method	Case	SIAE	MIN RMSE	Mean RMSE	MAX RMSE	STD of RMSE	Rank
MPSO [81]	SDM DDM Photowatt-PWP201 IFRI250-60	- - - -	7.7301×10^{-4} 7.4444×10^{-4} 2.0530×10^{-3} 7.5589×10^{-3}	- - - -	- - - -	- - - -	4
GCPSO [82]	SDM DDM Photowatt-PWP201 Sharp ND-R250A5	0.01763274 0.01637239 0.04400032 0.21867809	7.730063×10^{-4} 7.182745×10^{-4} 2.046535×10^{-3} 7.697717×10^{-3}	7.730063×10^{-4} 7.301380×10^{-4} 2.046535×10^{-3} 7.697717×10^{-3}	7.730065×10^{-4} 7.417141×10^{-4} 2.046536×10^{-3} 7.697719×10^{-3}	4.055839W-11 5.371802×10^{-6} 1.105194×10^{-10} 2.395516×10^{-10}	2.667
ELPSO [83]	SDM DDM STM6-40/36	- - -	7.7301×10^{-4} 7.4240×10^{-4} 2.1803×10^{-3}	7.7314×10^{-4} 7.5904×10^{-4} 2.2503×10^{-3}	7.7455×10^{-4} 7.9208×10^{-4} 3.7160×10^{-3}	3.4508×10^{-7} 9.4291×10^{-6} 2.9211×10^{-4}	N/A
SAIW-PSO [84]	SDM DDM	- -	7.73006×10^{-4} 7.41937×10^{-4}	7.73006×10^{-4} 7.42261×10^{-4}	7.73006×10^{-4} 7.54275×10^{-4}	5.49562×10^{-15} 1.41853×10^{-6}	N/A
DEDIWPSO [85]	SDM DDM Photowatt-PWP201 JKM330P-72	- - - -	7.730062×10^{-4} 7.182306×10^{-4} 2.03992×10^{-3} 4.3113×10^{-2}	7.730062×10^{-4} 7.187462×10^{-4} 2.03992×10^{-3} 4.3113×10^{-2}	7.730062×10^{-4} 7.318100×10^{-4} 2.03992×10^{-3} 4.3113×10^{-2}	5.18668×10^{-15} 2.486129×10^{-6} 2.995389×10^{-15} -	1.5
PPSO [86]	SDM DDM Photowatt-PWP201	- - -	9.8602×10^{-4} 9.8248×10^{-4} 2.4250×10^{-3}	9.8602×10^{-4} 9.8323×10^{-4} 2.4250×10^{-3}	9.8602×10^{-4} 9.8602×10^{-4} 2.4250×10^{-3}	7.0798×10^{-13} 1.3436×10^{-6} 2.8947×10^{-13}	5.167
PSO-ST [87]	SDM DDM Photowatt-PWP201 JKM330P-72	0.0214710 0.0212734 0.055499 -	7.73006×10^{-4} 7.183701×10^{-4} 2.03992×10^{-3} 4.3114×10^{-2}	7.73006×10^{-4} 7.187382×10^{-4} 2.03992×10^{-3} 4.3114×10^{-2}	7.73006×10^{-4} 7.218291×10^{-4} 2.03992×10^{-3} 4.3114×10^{-2}	5.18622×10^{-15} 1.318531×10^{-6} 2.91529×10^{-15} 6.2983×10^{-17}	1.833
PSOCS [88]	SDM DDM Photowatt-PWP201 SM55 KC200GT ST40	- - - - - -	9.8602×10^{-4} 9.8297×10^{-4} 2.4251×10^{-3} 3.8067×10^{-3} 2.5402×10^{-2} 7.3431×10^{-4}	9.8602×10^{-4} 1.0286×10^{-3} 2.4252×10^{-3} - - -	9.8603×10^{-4} 1.4133×10^{-4} 2.4282×10^{-3} - - -	1.7459×10^{-9} 9.9217×10^{-5} 5.9113×10^{-7} - - -	5.833

The "N/A" means that there is insufficient data to support an average algorithm ranking using the Friedman Test on the three cases: SDM, DDM, and Photowatt-PWP201.

3.4. ABCs

ABC was designed with several key members: a nectar source, nectar, and three types of bees [89]. The nectar amount from the flower represents the function value, and the food location means the solution. The nectar source and employed and onlooker bees are in quantity the same and the nectar source corresponds to the employed bees. Onlooker bees rely on nectar and employed bees to find flowers, and scout bees randomly fly to seek flowers near the hive [90].

In [91], the authors combined TLBO and ABC to design a method (TLABC) that included three search phases. The employed bee stage combined a teaching mechanism, the onlooker bee stage combined a learning mechanism, and the reconnaissance bee combined a generalized reversal mechanism. In [92], Wu et al. designed a new ABC (ABCTRR) by combining ABCs' exploiting capability with the trust-region reflective technique's exploiting capability. In [93], a new algorithm (IABC) was designed to solve ABC's early convergence issue by dividing the employed bee into two parts, one unchanged and the other searching the domain of the optimal global position. The identified parameters illustrated the high accuracy of IABC. For the integration of exploitation and exploration well, Tefek [94] combined ABC with a local search method to develop a new approach (ABC-Ls). Comparison revealed that ABC-Ls were more accurate, faster, and more stable. In [95], the authors compared ABC with PSO, showing that ABC outperformed PSO in all aspects of the results. In [96], a fitness distance balance mechanism was applied to TLABC to reconstruct a new method (FDB-TLABC). Experimental results confirmed the excellent performance of FDB-TLABC.

In Table 6, ABC-TRR has the least TNFES, followed by ABC, TLABC, IABC, ABC-Ls, and FDB-TLABC. There is an order-of-magnitude difference in resource consumption between ABC-TRR and the other variants of ABC. Table 7 compiles the experimental results. FDB-TLABC ranks first in combined MIN RMSE, followed by ABC-Ls, ABC-TRR, and TLABC. Therefore, achieving another increase in accuracy with less resource consumption for ABC is a priority for future research.

3.5. GWOs

GWO is a population-based metaheuristic with only two parameters [97]. Chase, encirclement, harassment, and attack are the hunt's four phases. Based on wolf rank, four types of wolves are included in GWO, with alpha being the strongest, followed by beta, delta, and omega. Wolves' mean solutions are in the solution space and are allowed to reposition. GWO only keeps the three optimal solutions, with other wolves responsible for position updating.

Table 6. ABCs' essential information and metrics.

Method	Main Contributors	Case	Algorithmic Parameter	Indicator	TNFES	Run
TLABC [91]	Chen et al., School of Electrical and Information Engineering, Jiangsu University	SDM DDM Photowatt-PWP201	NP = 50, $limit$ = 200, scale factor F = $rand$ (0, 1)	RMSE SIAE	50,000	30
ABC-TRR [92]	Wu et al., College of Physics and Information Engineering, Fuzhou University	SDM DDM Photowatt-PWP201	NP = 10, $limit$ = 10 NP = 10, $limit$ = 20 NP = 10, $limit$ = 10	RMSE SIAE	1000 5000 1000	1000
IABC [93]	Xu et al., College of Mathematics and Physics, Inner Mongolia University for Nationalities	SDM DDM	NP = 50, $limit$ = 50	RMSE IAE	50,000	-
ABC-Ls [94]	Tefek et al., Department of Computer Engineering, Osmaniye Korkut Ata University	SDM DDM Photowatt-PWP201	NP = 100, $limit$ = 250 NP = 100, $limit$ = 500 NP = 100, $limit$ = 250	RMSE IAE	50,000	30
Best-so-far ABC [95]	Garoudja et al., Centre de Développement des Technologies Avancées, CDTA	SDM LG395N2W	NP = 150, $limit$ = 750	RMSE	35,000	-
FDB-TLABC [96]	Duman et al., Electrical Engineering, Engineering and Natural Sciences Faculty, Bandirma Onyedi Eylul University	SDM DDM Photowatt-PWP201 STM6-40/36 STP6-120/36	NP = 50, $limit$ = 200, scale factor F = $rand$ (0, 1)	RMSE SIAE MIAE	50,000 70,000 50,000 50,000 50,000	51 51 51 - -

Table 7. ABCs' experiment results.

Method	Case	SIAE	MIN RMSE	Mean RMSE	MAX RMSE	STD of RMSE	Rank
TLABC [92]	SDM DDM Photowatt-PWP201	0.02152738 0.00135397 0.04880919	9.86022×10^{-4} 9.84145×10^{-4} 2.42507×10^{-3}	9.98523×10^{-4} 1.05553×10^{-3} 2.42647×10^{-3}	1.03970×10^{-3} 1.05553×10^{-3} 2.44584×10^{-3}	1.86022×10^{-5} 1.55034×10^{-4} 3.99568×10^{-6}	3.667
ABC-TRR [92]	SDM DDM Photowatt-PWP201	0.02152687 0.02127522 0.04892367	9.860219×10^{-4} 9.824849×10^{-4} 2.425075×10^{-3}	9.860219×10^{-4} 9.825556×10^{-4} 2.425075×10^{-3}	9.860219×10^{-4} 9.860219×10^{-4} 2.425075×10^{-3}	6.15×10^{-17} 4.95×10^{-7} 9.68×10^{-17}	3
IABC [93]	SDM DDM	- -	9.8602×10^{-4} 9.8248×10^{-4}	- -	- -	- -	N/A
ABC-Ls [94]	SDM DDM Photowatt-PWP201	- - -	9.8602×10^{-4} 9.8257×10^{-4} 2.4251×10^{-4}	- - -	- - -	- - -	2
Best-so-far ABC [95]	SDM LG395N2W	- -	0.027 0.013	- -	- -	- -	N/A
FDB-TLABC [96]	SDM DDM Photowatt-PWP201 STM6-40/36 STP6-120/36	0.017633 0.017001 - - -	7.7301×10^{-4} 7.4194×10^{-4} 2.054×10^{-3} 1.7319×10^{-3} 1.4251×10^{-2}	- - - - -	- - - - -	- - - - -	1.333

The "NA" means that there is insufficient data to support an average algorithm ranking using the Friedman Test on the three cases: SDM, DDM, and Photowatt-PWP201.

Vinod et al. [98] pioneered the use of GWO for the SDM, and the results showed that GWO had a high degree of accuracy. The study [99] found that more populations performed better, so a multi-group grey wolf optimizer (MGGWO) was developed. The results showed that MGGWO was excellent in speed and accuracy. A new GWO (OLBGWO) was designed in [100], which combined an orthogonal learning mechanism to improve the local exploration capability of GWO. OLBGWO's performance was evaluated in different PV models, and the results showed its excellent speed and accuracy. In [101], an improved GWO (I-GWO) was developed by introducing a hunting search mechanism based on dimensional learning. Ramadan et al. [102] introduced a domain search strategy to implement an improved GWO (IGWO) and demonstrated the algorithm's accuracy in two PV cases.

The relevant information and experimental results of the variants of GWO are summarized in Tables 8 and 9. I-GWO has the lowest resource consumption, followed by OLBGWO, GWO, MGGWO, and IGWO. Regarding overall accuracy ranking, OLBGWO is first and I-GWO is second. It is worth noting that MGGWO achieves a MIN RMSE of 4×10^{-4} on the SDM, a value not performed by any of the other algorithms counted. Variants of GWO use more computational resources, so there is much room for improvement in reducing the consumption of computational resources for GWO.

3.6. JAYAs

JAYA, which means victory in Sanskrit, combines survival of the fittest with the leader leading the population [103]. A key feature of JAYA is that there are no control parameters and no initial derivation information. When updating iteratively, the superior solution is approached quickly, and the inferior solution is moved away quickly.

Table 8. GWOs' essential information and metrics.

Method	Main Contributors	Case	Algorithmic Parameter	Indicator	TNFES	Run
GWO [98]	Vinod et al., Department of Electrical Engineering, Speciality of Optmization in Engineering, National Institute of Technology, Silchar, India	SDM	*NP* = 50	RMSE, IAE	50,000	-
MGGWO [99]	AlShabi et al., Mechanical and Nuclear Engineering Department, University of Sharjah, Sharjah, UAE	SDM	*NP* = 20	RMSE, MIAE	1,000,000	-
OLBGWO [100]	Xavier et al., Bule Hora University	SDM DDM Photowatt-PWP201 ST40 KC200GT	*NP* = 30, Orthogonal experiment levels: 3, Orthogonal experiment factors: 4	RMSE SIAE WRT	30,000	30
I-GWO [101]	Yesilbudak, Department of Electrical and Electronics Engineering, Faculty of Engineering and Architecture, Nevsehir Haci Bektas V eli University	SDM DDM TDM Photowatt-PWP201	*NP* = 15	RMSE IAE	25,000	50
IGWO [102]	Ramadan et al., Department of Electrical Engineering, Faculty of Engineering, Aswan University	TDM Photowatt-PWP201	*NP* = 1000, Iteration = 5000, *r1* = *rand*, *r2* = *rand*	RMSE	-	30

Table 9. GWOs' experiment results.

Method	Case	SIAE	MIN RMSE	Mean RMSE	MAX RMSE	STD of RMSE	Rank
GWO [98]	SDM	-	9.94378×10^{-4}	-	-	-	N/A
MGGWO [99]	SDM	-	4×10^{-4}	-	-	-	N/A
OLBGWO [100]	SDM DDM Photowatt-PWP201 ST40 KC200GT	- - - - -	9.86×10^{-4} 9.83×10^{-4} 2.4×10^{-3} 9.5666×10^{-4} 2.48×10^{-2}	9.86×10^{-4} 9.85×10^{-4} 2.4×10^{-3} - -	9.86×10^{-4} 9.86×10^{-4} 2.4×10^{-3} - -	1.4×10^{-8} 1.78×10^{-6} 2.4284×10^{-9} - -	1.333
I-GWO [101]	SDM DDM TDM Photowatt-PWP201	0.02152728 0.02127500 0.02128348 0.04892353	9.8602×10^{-4} 9.824852×10^{-4} 9.8251×10^{-4} 2.425075×10^{-3}	- - - -	- - - -	- - - -	1.667
IGWO [102]	TDM Photowatt-PWP201	- -	9.8331×10^{-4} 2.4276291×10^{-3}	9.84×10^{-4} 2.432×10^{-3}	9.85×10^{-4} 2.438×10^{-3}	6.60404×10^{-7} 5.26003×10^{-6}	N/A

The "N/A" means that there is insufficient data to support an average algorithm ranking using the Friedman Test on the three cases: SDM, DDM, and Photowatt-PWP201.

In [104], the authors designed an improved JAYA (IJAYA) that adaptively adjusted weights and optimized the algorithm performance using chaotic elite learning methods. IJAYA showed highly competitive performance in several PV models with excellent accuracy and reliability. An improved JAYA (EOJAYA) was developed in [105] by introducing an elite opposition mechanism to modify the update scheme. In [106], the Nelder-Mead algorithm was introduced to boost JAYA and this method's effectiveness was verified well in the SDM. In [107], a PGJAYA was designed to digitize the performance of individuals in a probabilistic manner as a guide to improve the search method. Adaptive chaotic perturbation techniques were employed to elevate the solution's overall quality. The PV model parameters estimated by PGJAYA proved its accuracy and robustness. Luu and Nguyen [108] introduced an adaptive population size mechanism to form a modified JAYA (MJA), and verified its performance and feasibility in the SDM and DDM. Jian et al. [109] developed a modified JAYA (LCJAYA) by introducing a logical chaotic mapping mechanism and a chaotic mutation mechanism in the update phase and search strategy of JAYA, respectively. LCJAYA's reliability and accuracy was verified in different PV cases. In [110], a simple improved JAYA (CLJAYA) was designed by integrating learning techniques, and its efficiency and accuracy was demonstrated in benchmark functions and PV models.

In [111], the authors improved a new JAYA (EJAYA) using an adaptive operator mechanism, a population size adjustment mechanism, and an opposition learning technique. The extraction of PV parameters demonstrated the effectiveness of EJAYA under different conditions. An enhanced chaotic JAYA (CJAYA) was developed in [112] by introducing an adaptive weighting strategy and three chaotic mechanisms including sine, tent, and logistic mappings. Saadaoui et al. [113] improved JAYA (MLJAYA) through three techniques: adaptive weighting, multiple learning, and chaotic perturbation. Jian and Cao [114] developed a chaotic second-order oscillation JAYA (CSOOJAYA) by using second-order oscillation factors, chaotic logistic mapping, and a mutation mechanism. The behavior of CSOOJAYA in solving the studied issue was demonstrated with good reliability and accuracy.

The essential information and experimental results of the variants of JAYA are summarized in Tables 10 and 11. Among them, the TNFES of EJAYA ranks first with 30,000, followed by CLJAYA, IJAYA, PGJAYA, LCJAYA, CJAYA, CSOOJAYA, EO-Jaya, and Jaya-NM. Regarding overall accuracy ranking, CLJAYA ranks first, followed by LCJAYA, EJAYA, MLJAYA, PGJAYA, CSOOJAYA, and IJAYA in order. In terms of computational resources, the JAYA variants consume more. Regarding specific values of FT, the difference between most variants is small, so further research on JAYA could go towards reducing the consumption of computational resources.

Table 10. JAYAs' essential information and metrics.

Method	Main Contributors	Case	Algorithmic Parameter	Indicator	TNFES	Run
IJAYA [104]	Yu et al., School of Electrical Engineering, Zhengzhou University	SDM DDM Photowatt-PWP201	$NP = 20$	RMSE IAE	50,000	30
EO-Jaya [105]	Wang et al., Department of Systems Engineering and Engineering Management, City University of Hong Kong	SDM DDM	$NP = 150$	RMSE	1,500,000	50
Jaya-NM [106]	Luo et al., School of Computer and Communication Engineering, University of Science and Technology Beijing (USTB)	SDM	$NP = 150$	RMSE	1,500,000	-
PGJAYA [107]	Yu et al., School of Electrical Engineering, Zhengzhou University	SDM DDM Photowatt-PWP201	$NP = 20$	RMSE	50,000	30
MJA [108]	Luu et al., Faculty of Electronics Technology, Industrial University of Ho Chi Minh City	SDM DDM	$NP^{init} = 10D$, $NP^{min} = D$, $r = rand\ (-0.5, 0.5)$,	RMSE	-	30
LCJAYA [109]	Jian et al., School of Optical Electrical and Computer Engineering, University of Shanghai for Science and Technology	SDM DDM Photowatt-PWP201	$NP = 20$	RMSE	50,000	30
CLJAYA [110]	Zhang et al., School of Electrical and Information Engineering, Tianjin University	SDM DDM Photowatt-PWP201	$NP = 20$	RMSE MIAE	20,000 50,000 30,000	-
EJAYA [111]	Yang et al., School of Computer Science, China University of Geosciences	SDM DDM Photowatt-PWP201 STM6-40/36 STP6-120/36	$NP = 30$, rate $Ra = 0.3$	RMSE WST	30,000	30
CJAYA [112]	Premkumar et al., Department of Electrical and Electronics Engineering, GMR Institute of Technology	SDM DDM STM6-40/36 STP6-120/36	$NP = 30$ $NP = 50$ $NP = 80$ $NP = 80$	RMSE IAE WST	50,000	30
MLJAYA [113]	Saadaoui et al., Laboratory of Materials and Renewable Energies, Faculty of Science, Ibn Zohr University	SDM DDM Photowatt-PWP201	$NP = 30$, $F = 3randn$	RMSE SIAE	-	30
CSOOJAYA [114]	Jian et al., School of Optical Electrical and Computer Engineering, University of Shanghai for Science and Technology	SDM DDM Photowatt-PWP201	$NP = 20$	RMSE IAE	50,000	30

Table 11. JAYAs' experiment results.

Method	Case	SIAE	MIN RMSE	Mean RMSE	MAX RMSE	STD of RMSE	Rank
IJAYA [104]	SDM DDM Photowatt-PWP201	- - -	9.8603×10^{-4} 9.8293×10^{-4} 2.4251×10^{-3}	9.9204×10^{-4} 1.0269×10^{-3} 2.4289×10^{-3}	1.0622×10^{-3} 1.4055×10^{-3} 2.4393×10^{-3}	1.4033×10^{-5} 9.8325×10^{-5} 3.7755×10^{-6}	6.5
EO-Jaya [105]	SDM DDM	- -	9.8603×10^{-4} 9.8262×10^{-4}	- -	- -	- -	N/A
Jaya-NM [106]	SDM	-	9.8602×10^{-4}	-	-	-	N/A
PGJAYA [107]	SDM DDM Photowatt-PWP201	- - -	9.8602×10^{-4} 9.8263×10^{-4} 2.425075×10^{-3}	9.8602×10^{-4} 9.8582×10^{-4} 2.425144×10^{-3}	9.8602×10^{-4} 9.9499×10^{-4} 2.426764×10^{-3}	1.4485×10^{-9} 2.5375×10^{-6} 3.071420×10^{-7}	3.833
MJA [108]	SDM DDM	- -	9.860218×10^{-4} 9.824848×10^{-4}	9.860218×10^{-4} 9.8260×10^{-4}	9.860218×10^{-4} 9.860218×10^{-4}	1.99×10^{-17} 6.46×10^{-7}	N/A
LCJAYA [109]	SDM DDM Photowatt-PWP201	- - -	9.8602×10^{-4} 9.8250×10^{-4} 2.425075×10^{-3}	9.8602×10^{-4} 9.8308×10^{-4} 2.425075×10^{-3}	9.8602×10^{-4} 9.8602×10^{-4} 2.425075×10^{-3}	5.6997×10^{-16} 1.3118×10^{-6} 2.415229×10^{-16}	3.5
CLJAYA [110]	SDM DDM Photowatt-PWP201	- - -	9.8602×10^{-4} 9.8249×10^{-4} 2.425075×10^{-3}	- - -	- - -	- - -	3.167
EJAYA [111]	SDM DDM Photowatt-PWP201 STM6-40/36 STP6-120/36	- - - - -	9.8602×10^{-4} 9.8248×10^{-4} 2.4251×10^{-3} 1.7298×10^{-3} 1.6601×10^{-2}	9.8602×10^{-4} 9.8448×10^{-4} 2.4251×10^{-3} 1.7298×10^{-3} 1.6601×10^{-2}	9.8602×10^{-4} 9.8602×10^{-4} 2.4251×10^{-4} 1.7298×10^{-3} 1.6601×10^{-2}	6.80×10^{-17} 1.51×10^{-6} 6.39×10^{-17} 1.47×10^{-17} 2.68×10^{-16}	3.5
CJAYA [112]	SDM DDM STM6-40/36 STP6-120/36	- - - -	9.8625×10^{-4} 1.0145×10^{-3} 1.7242×10^{-3} 1.6285×10^{-2}	9.8878×10^{-4} 1.01458×10^{-3} 1.7289×10^{-3} 1.6299×10^{-2}	9.8991×10^{-4} 1.0365×10^{-3} 1.7845×10^{-3} 1.6302×10^{-2}	4.5584×10^{-8} 7.5514×10^{-5} 1.4751×10^{-7} 3.2565×10^{-7}	N/A
MLJAYA [113]	SDM DDM Photowatt-PWP201	0.01781248 0.0176 0.04686375	9.8602×10^{-4} 9.8294×10^{-4} 2.4250748×10^{-3}	9.8602×10^{-4} 1.0618×10^{-3} 2.44395×10^{-3}	9.8602×10^{-4} 1.42102×10^{-3} 2.49419×10^{-3}	- - -	3.667
CSOOJAYA [114]	SDM DDM Photowatt-PWP201	- - -	9.860219×10^{-4} 9.824849×10^{-4} 2.425075×10^{-3}	9.860219×10^{-4} 9.824849×10^{-4} 2.425075×10^{-3}	9.860219×10^{-4} 9.824849×10^{-4} 2.425075×10^{-3}	4.717305×10^{-17} 5.576332×10^{-17} 2.699858×10^{-17}	3.833

The "N/A" means that there is insufficient data to support an average algorithm ranking using the Friedman Test on the three cases: SDM, DDM, and Photowatt-PWP201.

3.7. TLBOs

TLBO is a group metaheuristic developed based on the influence of teachers on students [115]. TLBO assumes that student outcomes are related to teacher competence. As the best in the group, the teacher teaches the students and raises the group's average achievement by a random factor. Students learn from each other at random coefficients during the learning phase and are led by the better of the two at random.

Chen et al. [116] suggested a generalized opposition-based learning mechanism for TLBO (GOTLBO). GOTLBO was demonstrated with excellent performance in benchmark functions and parameter extraction cases. To target different stages' effectiveness, Yu et al. [117] developed a self-adaptive TLBO (SATLBO) concerning elite learning mechanisms in the teacher stage and diverse learning mechanisms in the learner stage. SATLBO achieved competitive RMSE values in several PV models. Ramadan et al. [118] developed an enhanced TLBO (ETLBO) with controlled parameters replacing random parameter values and highlighted its effectiveness and competitiveness by extracting PV model parameters. Xiong et al. [21] developed an either/or TLBO (EOTLBO). To improve the generalizability of the method, EOTLBO replaced the mean with the learner median at the teacher stage. A random learner was added to the EOTLBO at the learner stage to improve the exploration capacity. The authors argued that it was inefficient for individuals to go through both teacher and learner stages, so EOTLBO implemented an either/or mechanism to choose one stage based on a chaotic map. EOTLBO showed excellent competitiveness, accuracy, and reliability. Abdel-Basset et al. [119] designed a modified TLBO (MTLBO). Individuals in both stages were divided into three strata of ground performance. Individual updates within each stratum did not interfere with each other. MTLBO was demonstrated with high accuracy in five PV models. Li et al. [120] developed an optimized TLBO (DMTLBO). The authors introduced the idea of dynamic self-adaption to the teacher stage and the idea of inter-comparison to the learner stage to further explore the capabilities of each stage. DMTLBO's accuracy, speed, and competitiveness were confirmed in different cases.

The essential information and experimental results of the TLBO variants are summarized in Tables 12 and 13. In the crucial information, GOTLBO has the least computational resources, followed by EOTLBO, SATLBO, MTLBO, DMTLBO, and ETLBO. In the accuracy ranking, EOTLBO comes first, followed by DMTLBO, MTLBO, and SATLBO. GOTLBO and ETLBO are not included because of missing values for some of the selected cases in the ranking. A direct comparison of the values in Table 13 reveals that the MIN RMSE of GOTLBO and ETLBO, which are early variants, struggle to outperform the other TLBO variants of recent years. An upward trend in the improvement of TLBO can be observed. However, the consumption of computational resources, unlike the development of accuracy, does not decrease significantly with the approaching number of years. Therefore, a reduction in the use of computational resources needs to be considered in future studies of TLBO.

Table 12. TLBOs' essential information and metrics.

Method	Main Contributors	Case	Algorithmic Parameter	Indicator	TNFES	Run
GOTLBO [116]	Chen et al., School of Electrical and Information Engineering, Jiangsu University	SDM DDM	NP = 20, SDM: Jr = 0.1, DDM: Jr = 0	RMSE	10,000 20,000	30
SATLBO [117]	Yu et al., Key Laboratory of Advanced Control and Optimization for Chemical Processes, Ministry of Education, East China University of Science and Technology	SDM DDM Photowatt-PWP201	NP = 40	RMSE	50,000	30
ETLBO [118]	Ramadan et al., Department of Electrical Engineering, Faculty of Engineering, Aswan University	SDM DDM STM6-40/36 STP6-120/36	NP = 200, Iteration = 5000,	RMSE IAE	-	-
EOTLBO [21]	Xiong et al., Guizhou Key Laboratory of Intelligent Technology in Power System, College of Electrical Engineering, Guizhou University	SDM DDM Photowatt-PWP201 Sharp ND-R250A5	NP = 50	RMSE WRT FT	20,000	50
MTLBO [119]	Abdel-Basset et al., Faculty of Computers and Informatics, Zagazig University	SDM DDM Photowatt-PWP201 STM6-40/36 STP6-120/36	NP = 50	RMSE	50,000	30
DMTLBO [120]	Li et al., Guizhou Key Laboratory of Intelligent Technology in Power System, College of Electrical Engineering, Guizhou University	SDM DDM Photowatt-PWP201 STM6-40/36 STP6-120/36	NP = 50	RMSE SIAE	50,000	30

Table 13. TLBOs' experiment results.

Method	Case	SIAE	MIN RMSE	Mean RMSE	MAX RMSE	STD of RMSE	Rank
GOTLBO [116]	SDM DDM	- -	9.87442×10^{-4} 9.83177×10^{-4}	1.33488×10^{-3} 1.24360×10^{-3}	1.98244×10^{-3} 1.78774×10^{-3}	2.99407×10^{-4} 2.09115×10^{-4}	N/A
SATLBO [117]	SDM DDM Photowatt-PWP201	- - -	9.86022×10^{-4} 9.828037×10^{-4} 2.425075×10^{-3}	9.87795×10^{-4} 9.981111×10^{-4} 2.425428×10^{-3}	9.94939×10^{-6} 1.047045×10^{-3} 2.429130×10^{-3}	2.30015×10^{-6} 1.951533×10^{-5} 7.410517×10^{-7}	3.667
ETLBO [118]	SDM DDM STM6-40/36 STP6-120/36	- - - -	9.86022×10^{-4} 9.8241×10^{-4} 1.7759×10^{-3} 1.6172×10^{-2}	- - - -	- - - -	- - - -	N/A
EOTLBO [21]	SDM DDM Photowatt-PWP201 Sharp ND-R250A5	- - - -	$9.86021878 \times 10^{-4}$ $9.82484852 \times 10^{-4}$ $2.42507487 \times 10^{-3}$ $1.11833356 \times 10^{-2}$	$9.86021878 \times 10^{-4}$ $9.84733697 \times 10^{-4}$ $2.42507487 \times 10^{-3}$ $1.11839904 \times 10^{-2}$	$9.86021878 \times 10^{-4}$ $9.89424104 \times 10^{-4}$ $2.42507487 \times 10^{-3}$ $1.12154997 \times 10^{-2}$	$4.12665088 \times 10^{-17}$ $1.69176118 \times 10^{-6}$ $3.61995116 \times 10^{-17}$ $4.54767027 \times 10^{-6}$	1.667
MTLBO [119]	SDM DDM Photowatt-PWP201 STM6-40/36 STP6-120/36	- - - - -	9.860219×10^{-4} 9.824849×10^{-4} 2.4250749×10^{-3} 1.7298137×10^{-3} $1.66006031 \times 10^{-2}$	9.860219×10^{-4} 9.824855×10^{-4} 2.4250749×10^{-3} 1.7298137×10^{-3} $1.66006031 \times 10^{-2}$	9.860219×10^{-4} 9.825026×10^{-4} 2.4250749×10^{-3} 1.7298137×10^{-3} $1.66006031 \times 10^{-2}$	$1.9292748 \times 10^{-17}$ 3.3000000×10^{-9} $1.3070107 \times 10^{-17}$ $5.9363718 \times 10^{-18}$ $8.0041380 \times 10^{-17}$	2.667
DMTLBO [120]	SDM DDM Photowatt-PWP201 STM6-40/36 STP6-120/36	0.0178 0.0176 0.0411 0.0215 0.2741	9.8602×10^{-4} 9.8248×10^{-4} 2.4251×10^{-3} 1.7298×10^{-3} 1.6601×10^{-2}	9.8602×10^{-4} 9.8406×10^{-4} 2.4251×10^{-3} 1.7298×10^{-3} 1.6601×10^{-2}	9.8602×10^{-4} 9.8638×10^{-4} 2.4251×10^{-3} 1.7298×10^{-3} 1.6601×10^{-2}	2.07×10^{-17} 1.53×10^{-6} 2.15×10^{-17} 5.74×10^{-14} 4.55×10^{-10}	2

The "N/A" means that there is insufficient data to support an average algorithm ranking using the Friedman Test on the three cases: SDM, DDM, and Photowatt-PWP201.

3.8. WOAs

WOA consists of an attack prey phase responsible for exploitation and a search prey phase responsible for exploration [121,122]. The bubble net attack consists of two mechanisms, i.e., encircling prey and spiral update position, both of which have the same probability of being selected. The encircling prey mechanism can determine any position between the present and best individuals within a specific range related to the parameter a, which decreases from 2 to 1 as the optimization proceeds. In the spiral position update, the individual's position is determined by the spiral equation between the whale and the prey. In the search phase, individuals are updated similarly to the encircling prey mechanism, except that a random individual replaces the optimal individual.

An improved WOA (IWOA) was developed in [123] to address the premature convergence of WOA. IWOA adjusted the encircling prey mechanism and modified the updating search phase to enhance the exploration, diversity, and robustness. Experiments in different PV models showed that IWOA extracted parameters with fast convergence, high quality, good robustness, and competitiveness. In [124], Elazab et al. pioneered the application of WOA to this studied problem. Comparisons with other algorithms demonstrated that WOA can fit PV data more accurately. To further enhance the ability of WOA to cope with the studied problem, Xiong et al. [18] developed a variant of WOA (MCSWOA) by modifying the search strategy of WOA using DE's mutation equation. A crossover operator was designed to improve the algorithm's applicability in different dimensions. A selection operator was designed to ensure that the optimization process would not worsen at any time. The perfect convergence curves, RMSE values, SIAE values, and ranking indicated that MCSWOA was characterized by high accuracy, competitiveness, and fast convergence. Pourmousa et al. [125] designed a Springy WOA (SWOA) by adding a deletion stage to the WOA. Peng et al. [126] developed a new approach (ISNMWOA) by combining the Nelder-Mead simplex technique with WOA. The results demonstrated that ISNMWOA's performance was significantly higher than WOA and it ran faster than other high-performance methods.

The essential information and experimental results of the variants of GWO are summarized in Tables 14 and 15. WOA has the least computational resources, followed by ISNMWOA, MCSWOA, IWOA, and SWOA, in order. In Table 15, SWOA has the highest overall MIN RMSE ranking, followed by ISNMWOA, IWOA, and MCSWOA. SWOA has high accuracy but consumes a lot of computational resources, with 5000 iterations at a population size of 30. The accuracy of ISNMWOA is close to that of SWOA, and TNFES at 20,000 is much lower than SWOA but still needs further improvement.

Table 14. WOAs' essential information and metrics.

Method	Main Contributors	Case	Algorithmic Parameter	Indicator	TNFES	Run
WOA [124]	Elazab et al., Electrical Power and Machines Department, Faculty of Engineering, Ain Shams University	KC200GT	NP = 30, Iteration = 500,	-	15,000	-
IWOA [123]	Xiong et al., Guizhou Key Laboratory of Intelligent Technology in Power System, College of Electrical Engineering, Guizhou University	SDM DDM Photowatt-PWP201	NP = 50, Iteration = 2000,	RMSE SIAE WRT, FT	-	50
MCSWOA [18]	Xiong et al., Guizhou Key Laboratory of Intelligent Technology in Power System, College of Electrical Engineering, Guizhou University	SDM DDM Photowatt-PWP201 STM6-40/36 STP6-120/36 Sharp ND-R250A5	NP = 50	RMSE SIAE FT	50,000	50
SWOA [125]	Pourmousa et al., Department of Electrical Engineering, Iran University of Science and Technology	SDM DDM TDM Photowatt-PWP201	NP = 30, Iteration = 5000,	RMSE IAE	-	30
ISNMWOA [126]	Peng et al., Department of Computer Science and Artificial Intelligence, Wenzhou University	SDM DDM TDM Photowatt-PWP201	NP = 30	RMSE SIAE	20,000	-

Table 15. WOAs' experiment results.

Method	Case	SIAE	MIN RMSE	Mean RMSE	MAX RMSE	STD of RMSE	Rank
IWOA [123]	SDM DDM Photowatt-PWP201	0.01770338 0.01735511 0.04176116	9.860219×10^{-4} 9.824849×10^{-4} 2.425075×10^{-3}	9.860219×10^{-4} 9.826140×10^{-4} 2.425075×10^{-3}	9.860219×10^{-4} 9.860219×10^{-4} 2.425075×10^{-3}	5.12×10^{-16} 9.86×10^{-5} 2.90×10^{-17}	2.667
MCSWOA [18]	SDM DDM Photowatt-PWP201 STM6-40/36 STP6-120/36 Sharp ND-R250A5	0.01770381 0.01730633 0.04178694 0.02177346 0.27780418 0.21759970	9.8602×10^{-4} 9.8250×10^{-4} 2.4251×10^{-3} 1.7298×10^{-3} 1.6601×10^{-2} 1.1183×10^{-2}	9.8602×10^{-4} 1.0078×10^{-3} 2.4252×10^{-3} 1.7311×10^{-3} 1.6632×10^{-2} 1.1187×10^{-2}	9.8602×10^{-4} 1.1903×10^{-3} 2.4270×10^{-3} 1.7364×10^{-3} 1.6741×10^{-2} 1.1244×10^{-2}	4.8373×10^{-10} 3.7264×10^{-5} 3.2927×10^{-7} 1.0774×10^{-6} 2.6486×10^{-5} 9.1358×10^{-6}	3.167
SWOA [125]	SDM DDM TDM Photowatt-PWP201	- - - -	9.8602×10^{-4} 9.8249×10^{-4} 9.8033×10^{-4} 2.4250×10^{-3}	9.8602×10^{-4} 9.8250×10^{-4} 9.8051×10^{-4} 2.4250×10^{-3}	9.8602×10^{-4} 9.8251×10^{-4} 9.8154×10^{-4} 2.4250×10^{-3}	- - - -	2
ISNMWOA [126]	SDM DDM TDM Photowatt-PWP201	0.021527008 0.021275213 0.021275347 0.048923833	9.8602×10^{-4} 9.8248×10^{-4} 9.8248×10^{-4} 2.4251×10^{-3}	- - - -	- - - -	- - - -	2.167

3.9. Hybrids

The above methods used for the studied problem are partially dominated by a single metaheuristic algorithm. In addition to them, hybrid approaches that combine two and more metaheuristics are also popular for solving this problem. The motivation behind the hybrid approaches is integrating diverse features of different algorithms to equilibrate the global and local search abilities.

In [127], Xiong et al. devised an approach (DE/WOA) that took full advantages of DE and WOA to balance diversity and convergence. Long et al. [128] developed an approach (GWOCS) introducing the opposing learning mechanism of cuckoo search (CS) for the three optimal individuals preserved by GWO to achieve improved performance. The results of benchmark functions and PV models supported the authors' expectations of performance improvement. Rizk et al. [129] developed a new method (PSOGWO) by mixing GWO and PSO to make full use of their exploration and exploitation advantages. Different PV models demonstrated the excellent performance of PSOGWO. Li et al. [130] designed a DE-based adaptive TLBO (ATLDE) by mixing DE with TLBO and adjusting the teaching and learning stages using a ranking probability mechanism. Experimental results supported ATLDE's competitiveness. In [131], the authors effectively combined DE with Harris Hawks Optimization (HHO) to form a new method (HHODE), and demonstrated the effectiveness of the improvement using RMSE values for the extracted PV parameters. Yu et al. [132] devised a new method (HAJAYADE) by replacing the two parameters of JAYA adaptively. Then, the method combined DE and introduced a mutational operator and an adaptive chaos mechanism to ensure its performance. Devarapalli et al. [133] improved the updated approach of a hybrid of GWO and sine cosine algorithm (HGWOSCA) to gain an enhanced method (EHGWOSCA). Singh et al. [47] hybridized the Dingo Optimizer and PSO to form a new hybrid algorithm (HPSODOX) and developed a four-diode PV model to reveal HPSODOX's performance. The results supported the validity of the algorithm improvement. Weng et al. [134] integrated a Backtracking Search Algorithm with TLBO to form a new method (TLBOABC) and verified the method's effectiveness well.

The essential information and experimental results of the hybrid methods are summarized in Tables 16 and 17. TLBOBSA has the lowest computational resource consumption, followed by ATLDE, DE/WOA, GWOCS, and HAJAYADE. TLBOBSA has the highest overall ranking for MIN RMSE, followed by DE/WOA, HAJAYADE, and GWOCS. TLBOBSA ranks the highest in resource consumption and accuracy, indicating that a suitable hybrid scheme can achieve significant performance. It should be noted that the MIN RMSE of HPSODOX, although very small, needs more basic information, and there are no repeated runs for the experiment, so it is impossible to evaluate the performance of this method for the time being.

3.10. Others

New methods usually lead to breakthroughs in specific problems, since they bring different search mechanisms. Therefore, researchers favor novel approaches and their variants in exploring the PV model parameter extraction, and have provided some new approaches.

Naeijian et al. [135] developed a Whippy Harris Hawk Optimization (WHHO) that handled the worst individual by adding elimination cycles to improve all-around performance. The simulation results demonstrated the fast convergence of WHHO and the high robustness and accuracy for the extracted parameters. Xiong et al. [4] used a Gaining-Sharing Knowledge-based algorithm (GSK) for the issue addressed in this work for the first time. They demonstrated the high accuracy, robustness, and competitiveness of GSK in different PV models. Sallam et al. [136] developed an improved GSK (IGSK) using a boundary constraint processing mechanism, a linear population size reduction technique, and knowledge rate adaptive technology. Xiong et al. [137] applied Supply and Demand Based Optimization (SDO) and pioneered a comparison between SDO and several advanced methods in extracting PV model parameters, which powerfully demonstrated the feasibility and competitiveness of SDO. Diad et al. [138] used a Tree Growth Algorithm (TGA) to tackle the issue, and the RMSE values showed the TGA's good accuracy. Abbassi et al. [139] provided PV model parameters extracted by a Salp Swarm Algorithm (SSA) and demonstrated its accuracy and competitiveness with multiple metrics. Sharma et al. [140] solved this problem using Tunicate Swarm Algorithm (TSA) and verified TSA's accuracy, feasibility, and competitiveness with simulations. Gupta et al. [141] designed a chaotic TSA (CTSA) to tackle the issue, and the results supported its accuracy and competitiveness. Ramadan et al. [142] developed Chaotic Game Optimization (CGO) for the issue and confirmed its good performance. Long et al. [143] designed a Hybrid Seagull Optimization (HSOA) with three mechanisms, differential mutation, memory-guided and non-linear control, and tested it in different PV models. Shaban et al. [144] employed Rungakuta Optimizer (RUN) to tackle the issue. The simulation results demonstrated RUN's excellent competitiveness, convergence, and robustness. In [145], the authors used a Flower Pollination Optimization Algorithm (FPOA) for the TDM's parameters with industrial samples. The results supported the high-performance of FPOA in the TDM. In [146], the authors used the Symbiotic Organisms Search (SOS) method to tackle the issue. The results powerfully demonstrated the superiority of SOS.

Table 16. Hybrids' essential information and metrics.

Method	Main Contributors	Case	Algorithmic Parameter	Indicator	TNFES	Run
DE/WOA [127]	Xiong et al., Guizhou Key Laboratory of Intelligent Technology in Power System, College of Electrical Engineering, Guizhou University	SDM DDM Photowatt-PWP201	NP = 40, F = $rand$ (0.1, 1), CR = $rand$ (0, 1)	RMSE MIAE	50,000	50
GWOCS [128]	Long et al., Key Laboratory of Economics System Simulation, Guizhou University of Finance and Economics	SDM DDM Photowatt-PWP201 STM6-40/36	NP = 30	RMSE IAE FT	50,000	30
PSOGWO [129]	Rezk et al., College of Engineering at Wadi Addawaser, Prince Sattam Bin Abdulaziz University	Photowatt-PWP201 STE4/100 FSM	Iteration = 1200 Iteration = 6000 Iteration = 2000	RMSE MIAE	-	-
ATLDE [130]	Li et al., School of Computer Science, China University of Geosciences	SDM DDM STM6-40/36 STP6-120/36	NP = 50, F = $rand$, CR = 0.9	RMSE SIAE WRT	30,000	30
HHODE [131]	Ndi et al., Technology and Applied Sciences Laboratory, University of Douala	SDM DDM	Iteration = 3000	RMSE	-	20
HAJAYADE [132]	Yu et al., School of Management Science and Engineering, Nanjing University of Information Science and Technology	SDM DDM Photowatt-PWP201 STM6-40/36 STP6-120/36	NP = 20, CR = 0.5	RMSE WST	50,000	30
EHGWOSCA [133]	Devarapalli et al., Department of EEE, Lendi Institute of Engineering and Technology	SDM DDM Shell S75 Shell CS6K280M Shell ST40	Iteration = 500	ERR	-	30
HPSODOX [47]	Singh et al., Electrical and Instrumentation Engineering Department, Thapar Institute of Engineering and Technology	SDM DDM TDM FDM	-	RMSE FT	-	-
TLBOBSA [134]	Weng et al., Department of Computer Science and Artificial Intelligence, Wenzhou University	SDM DDM TDM Photowatt-PWP201	NP = 30	RMSE SIAE	20,000	30

Table 17. Hybrids' experiment results.

Method	Case	SIAE	MIN RMSE	Mean RMSE	MAX RMSE	STD of RMSE	Rank
DE/WOA [127]	SDM	0.01770392	9.860219×10^{-4}	9.860219×10^{-4}	9.860219×10^{-4}	3.545178×10^{-17}	2.333
	DDM	0.01731808	9.824849×10^{-4}	9.829703×10^{-4}	9.860377×10^{-4}	9.152178×10^{-7}	
	Photowatt-PWP201	0.04178725	2.425075×10^{-3}	2.425092×10^{-3}	2.425442×10^{-3}	6.270718×10^{-8}	
GWOCS [128]	SDM	-	9.8607×10^{-4}	9.8874×10^{-4}	9.9095×10^{-4}	2.4696×10^{-6}	3.5
	DDM	-	9.8334×10^{-4}	9.9411×10^{-4}	1.0017×10^{-3}	9.5937×10^{-6}	
	Photowatt-PWP201	-	2.4251×10^{-3}	2.4261×10^{-3}	2.4275×10^{-3}	1.1967×10^{-6}	
	STM6-40/36	-	1.7337×10^{-3}	1.7457×10^{-3}	1.7528×10^{-3}	1.0447×10^{-5}	
PSOGWO [129]	Photowatt-PWP201	0.06292	3.06×10^{-3}	-	-	-	N/A
	STE4/100	0.00384	3.0574×10^{-4}	-	-	-	
	FSM	0.16023	9.14×10^{-3}	-	-	-	
ATLDE [130]	SDM	0.0177	9.8602×10^{-4}	9.8602×10^{-4}	9.8602×10^{-4}	2.44×10^{-17}	N/A
	DDM	0.0173	9.8218×10^{-4}	9.8372×10^{-4}	9.8603×10^{-4}	1.37×10^{-6}	
	STM6-40/36	0.0218	1.7298×10^{-3}	1.7298×10^{-3}	1.7298×10^{-3}	8.22×10^{-18}	
	STP6-120/36	0.2780	1.6601×10^{-2}	1.6601×10^{-2}	1.6601×10^{-2}	1.02×10^{-16}	
HHODE [131]	SDM	-	1.4664×10^{-3}	-	-	-	N/A
	DDM	-	1.5978×10^{-3}	-	-	-	
HAJAYADE [132]	SDM	-	9.8602×10^{-4}	9.8602×10^{-4}	9.8602×10^{-4}	0	2.833
	DDM	-	9.8294×10^{-4}	9.8641×10^{-4}	9.96×10^{-4}	2.8534×10^{-6}	
	Photowatt-PWP201	-	2.4251×10^{-3}	2.4251×10^{-3}	2.4251×10^{-3}	3.2215×10^{-15}	
	STM6-40/36	-	1.7298×10^{-3}	1.7298×10^{-3}	1.7298×10^{-3}	3.6569×10^{-16}	
	STP6-120/36	-	1.6601×10^{-2}	1.6601×10^{-2}	1.6606×10^{-2}	9.2421×10^{-7}	
HPSODOX [47]	SDM	-	6.4923×10^{-9}	-	-	-	N/A
	DDM	-	6.5120×10^{-9}	-	-	-	
	TDM	-	6.5424×10^{-9}	-	-	-	
	FDM	-	6.5656×10^{-9}	-	-	-	
TLBOBSA [134]	SDM	0.021526887	9.86902×10^{-4}	9.8602×10^{-4}	9.8603×10^{-4}	5.64965×10^{-10}	1.667
	DDM	0.021312577	9.8155×10^{-4}	1.1334×10^{-3}	2.2181×10^{-3}	3.0012×10^{-4}	
	TDM	0.021263898	9.82553×10^{-4}	1.2081×10^{-3}	3.0608×10^{-3}	4.9433×10^{-4}	
	Photowatt-PWP201	0.048923676	2.42507×10^{-3}	2.42535×10^{-3}	2.43167×10^{-3}	1.21238×10^{-6}	

The "N/A" means that there is insufficient data to support an average algorithm ranking using the Friedman Test on the three cases: SDM, DDM, and Photowatt-PWP201.

Most of the above methods are applications of newly proposed metaheuristics in recent years, and their essential information and experimental results are summarized in Tables 18 and 19. SSA has the smallest TNFES, followed by IGSK, RUN, GSK, SDO, TSA, HSOA, CTSA, SOS, WHHO, and TGA. WHHO and TGA achieve the same combined MIN RMSE ranking, followed by GSK, IGSK, HSOA, and SOS, in that order. It is worth noting that RUN, as the original algorithm, obtained more accurate parameter values with not many computational resources. TGA achieved the most efficient MIN RMSE values for DDM and TDM, and GSK received enough accuracy to compare with many advanced algorithms with not many computational resources. This suggests that exploring the application of new methods may make it easier to achieve a solution to the issue.

Table 18. Other methods' essential information and metrics.

Method	Main Contributors	Case	Algorithmic Parameter	Indicator	TNFES	Run
WHHO [135]	Naeijian et al., Department of Electrical Engineering, Babol Noshirvani University of Technology	SDM DDM TDM Photowatt-PWP201	NP = 30, Iteration = 5000,	RMSE IAE	-	30
GSK [4]	Xiong et al., Guizhou Key Laboratory of Intelligent Technology in Power System, College of Electrical Engineering, Guizhou University	SDM DDM Photowatt-PWP201 STM6-40/36 STP6-120/36	NP = 30, k_r = 0.9, k_f = 0.5, K = 10, p = 0.1	RMSE SIAE FT	30,000 50,000 30,000 30,000 30,000	30
IGSK [136]	Sallam et al., The Faculty of Computers and Information, Zagazig University	SDM DDM Photowatt-PWP201 STM6-40/36 STP6-120/36	NP^{init} = 25, k_r = 0.9, k_f = 0.5, K = 10, p = 0.1	RMSE WST	10,000 20,000 10,000 15,000 15,000	30
SDO [137]	Xiong et al., Guizhou Key Laboratory of Intelligent Technology in Power System, College of Electrical Engineering, Guizhou University	SDM DDM PVM 752 GaAs STM6-40/36 STP6-120/36	NP = 20	RMSE SIAE WRT FT	50,000	50
TGA [138]	Diab et al., Electrical Engineering Department, Faculty of Engineering, Minia University	SDM DDM TDM PVM 752 GaAs Photowatt-PWP201 STE 20/100	NP = 500, Iteration = 500,	RMSE	-	-
SSA [139]	Abbassi et al., University of Kairouan, Institute of Applied Sciences and Technology of Kasserine (ISSATKas)	TITAN-12-50	NP = 30, Iteration = 100,	RMSE IAE	-	30
TSA [140]	Sharma et al., Research and Development Department, University of Petroleum and Energy Studies	Photowatt-PWP201	NP = 30	RMSE, SIAE, FT	50,000	30
CGO [142]	Ramadan et al., Department of Electrical Engineering, Faculty of Engineering, Aswan University	TDM Photowatt-PWP201	Iteration = 1000	RMSE IAE	-	15
HSOA [143]	Long et al., Key Laboratory of Economics System Simulation, Guizhou University of Finance and Economics	SDM DDM Photowatt-PWP201	NP = 30, f_{cmax} = 2, f_{cmin} = 0, F = 0.5	RMSE SIAE FT	50,000	20
RUN [144]	Shaban et al., Faculty of Computers and Information, Minia University	SDM DDM TDM	NP = 30, Iteration = 1000, a = 20, b = 12	RMSE IAE FT	-	30
FPOA [145]	Chellaswamy et al., Department of ECE, Lords Institute of Engineering and Technology	Sample2, Sample5	β = 1.45, S_p = 0.85	MIAE	-	-
CTSA [141]	Gupta et al., Electrical and Instrumentation Engineering Department, Thapar Institute of Engineering and Technology	DDM TDM	NP = 50, Iteration = 1000	RMSE SIAE	-	-
SOS [146]	Xiong et al., Guizhou Key Laboratory of Intelligent Technology in Power System, College of Electrical Engineering, Guizhou University	SDM DDM Photowatt-PWP201	NP = 50	RMSE SIAE WRT	50,000	50

Table 19. Other methods' experiment results.

Method	Case	SIAE	MIN RMSE	Mean RMSE	MAX RMSE	STD of RMSE	Rank
WHHO [135]	SDM	-	9.8602×10^{-4}	9.8602×10^{-4}	9.8602×10^{-4}	-	2.667
	DDM	-	9.82487×10^{-4}	9.8249×10^{-4}	9.8250×10^{-4}	-	
	TDM	-	9.80751×10^{-4}	9.8085×10^{-4}	9.8149×10^{-4}	-	
	Photowatt-PWP201	-	2.4250×10^{-3}	2.4250×10^{-3}	2.4250×10^{-3}	-	
GSK [4]	SDM	0.0174	9.8602×10^{-4}	9.8602×10^{-4}	9.8602×10^{-4}	2.18×10^{-17}	3
	DDM	0.0175	9.8248×10^{-4}	9.8280×10^{-4}	9.8602×10^{-4}	8.72×10^{-7}	
	Photowatt-PWP201	0.0411	2.4251×10^{-3}	2.4251×10^{-3}	2.4251×10^{-3}	1.04×10^{-9}	
	STM6-40/36	0.0218	1.7298×10^{-3}	1.7298×10^{-3}	1.7298×10^{-3}	6.25×10^{-18}	
	STP6-120/36	0.2829	1.6601×10^{-2}	1.6601×10^{-2}	1.6601×10^{-2}	1.44×10^{-16}	
IGSK [136]	SDM	-	9.8602188×10^{-4}	9.8602188×10^{-4}	9.8602188×10^{-4}	$3.5821018 \times 10^{-17}$	3.33
	DDM	-	9.8248485×10^{-4}	9.8272774×10^{-4}	9.8602188×10^{-4}	8.9578942×10^{-7}	
	Photowatt-PWP201	-	2.4250749×10^{-3}	2.4250749×10^{-3}	2.4250749×10^{-3}	$2.9226647 \times 10^{-17}$	
	STM6-40/36	-	1.7298137×10^{-3}	1.7298137×10^{-3}	1.7298137×10^{-3}	$7.0155794 \times 10^{-18}$	
	STP6-120/36	-	1.6600603×10^{-2}	1.6600603×10^{-2}	1.6600603×10^{-2}	$1.7069489 \times 10^{-16}$	
SDO [137]	SDM	0.01770381	9.8602×10^{-4}	9.8603×10^{-4}	9.8616×10^{-4}	2.5141×10^{-8}	N/A
	DDM	0.01730620	9.8250×10^{-4}	9.8822×10^{-4}	1.0271×10^{-3}	8.8518×10^{-6}	
	PVM 752 GaAs	0.00593491	2.3487×10^{-4}	3.1727×10^{-4}	3.7700×10^{-4}	2.7687×10^{-5}	
	STM6-40/36	0.02177419	1.7298×10^{-3}	1.7703×10^{-3}	1.9500×10^{-3}	4.5108×10^{-5}	
	STP6-120/36	0.27797428	1.6601×10^{-2}	1.6683×10^{-2}	1.6866×10^{-2}	7.1751×10^{-5}	
TGA [138]	SDM	-	$9.750530454421328 \times 10^{-4}$	-	-	-	2.667
	DDM	-	$8.488244232381 \times 10^{-4}$	-	-	-	
	TDM	-	$8.251052783901371 \times 10^{-4}$	-	-	-	
	PVM 752 GaAs	-	$9.037521972258222 \times 10^{-4}$	-	-	-	
	Photowatt-PWP201	-	$3.819491771269 \times 10^{-3}$	-	-	-	
	STE 20/100	-	$9.28071173 \times 10^{-4}$	-	-	-	
SSA [139]	TITAN-12-50(366)	-	2.9681 × 10−04	-	-	-	N/A
	TITAN-12-50(810.2)	-	1.5777 × 10−06	-	-	-	
TSA [140]	Photowatt-PWP201	0.0594	5.06×10^{-4}	1.45×10^{-3}	2.34×10^{-2}	1.25×10^{-3}	N/A
CGO [142]	TDM	-	9.82×10^{-4}	9.82×10^{-4}	9.82×10^{-4}	1.24841×10^{-9}	N/A
	Photowatt-PWP201	-	2.425075×10^{-3}	2.425092×10^{-3}	2.4251×10^{-3}	1.44688×10^{-8}	
HSOA [143]	SDM	0.0177065	9.8602×10^{-4}	1.0479×10^{-3}	1.1683×10^{-3}	5.3832×10^{-5}	4
	DDM	0.017402	9.8376×10^{-4}	1.1175×10^{-3}	1.7642×10^{-3}	1.9107×10^{-4}	
	Photowatt-PWP201	0.041788	2.4251×10^{-3}	2.4251×10^{-3}	2.4253×10^{-3}	4.1556×10^{-8}	
RUN [144]	SDM	-	9.86242×10^{-4}	1.479894×10^{-3}	2.444572×10^{-3}	4.30699×10^{-4}	N/A
	DDM	-	9.87168×10^{-4}	1.481762×10^{-3}	2.947571×10^{-3}	5.14117×10^{-4}	
	TDM	-	9.89133×10^{-4}	1.581238×10^{-3}	6.239595×10^{-3}	1.078762×10^{-3}	
CTSA [141]	DDM	0.2621	1.0239×10^{-8}	2.1185×10^{-8}	9.6017×10^{-8}	3.9865×10^{-8}	N/A
	TDM	0.0075	1.0036×10^{-6}	3.4906×10^{-6}	9.4766×10^{-6}	2.7057×10^{-6}	
SOS [146]	SDM	0.0181	9.8609×10^{-4}	1.0245×10^{-3}	1.1982×10^{-3}	5.2184×10^{-5}	5.333
	DDM	0.0182	9.8518×10^{-4}	1.0627×10^{-3}	1.3498×10^{-3}	9.6141×10^{-5}	
	Photowatt-PWP201	0.0421	2.4251×10^{-3}	2.4361×10^{-3}	2.5103×10^{-3}	1.7503×10^{-5}	

The "N/A" means that there is insufficient data to support an average algorithm ranking using the Friedman Test on the three cases: SDM, DDM, and Photowatt-PWP201.

4. Whole Analysis and Research Prospects

This section presents metaheuristic methods in solving the studied problem. We collect their data for an overall analysis and give some research prospects.

4.1. Data Analysis

In the third part, the final results of many methods are relatively convergent. For SDM, the RMSE is mainly distributed around 9.8206×10^{-4} and the rest is concentrated around 7.7301×10^{-4}. The DDM's primary distribution is around 9.8248×10^{-4}, with a secondary allocation of 7.42×10^{-4} to 7.1823×10^{-4}. For the TDM, the main distribution is between 9.8331×10^{-4} and 9.8033×10^{-4}, with higher precision than the main distribution interval, being 8.2511×10^{-4} for TGA and 6.5424×10^{-9} for HPSODOX. For Photowatt-PWP201, the main distribution is around 2.4251×10^{-3}, the secondary distribution is around 2.0399×10^{-3}, and the best-performing TSA reaches 5.06×10^{-4}. STM6-40/36 is mainly distributed at 1.7298×10^{-3}. STP6-120/36 is primarily distributed at 1.6601×10^{-2} nearby; the best-performing FDB-TLABC achieved 1.4251×10^{-2}. However, the different approaches rarely use the same cases and evaluation indicators, and the results may differ between models. Therefore, some well-performed variants of metaheuristics that used the RMSE indicators are selected for further comparison in Table 20, i.e., ABC-TRR, RLDE, OLBWOA, CSOOJAYA, DEDIWPSO, EOTLBO, IWOA, TLBOBSA, IGSK, HSOA, and SOS.

Table 20. Various methods' RMSE results.

Method	Case	MIN RMSE	Mean RMSE	MAX RMSE	STD of RMSE	Rank
ABC-TRR [92]	SDM DDM Photowatt-PWP201	9.860219×10^{-4} 9.824849×10^{-4} 2.425075×10^{-3}	9.860219×10^{-4} 9.825556×10^{-4} 2.425075×10^{-3}	9.860219×10^{-4} 9.860219×10^{-4} 2.425075×10^{-3}	6.15×10^{-17} 4.95×10^{-7} 9.68×10^{-17}	5.958
RLDE [41]	SDM DDM Photowatt-PWP201	9.8602×10^{-4} 9.8248×10^{-4} 2.4251×10^{-3}	9.8602×10^{-4} 9.8695×10^{-4} 2.4251×10^{-3}	9.8602×10^{-4} 9.8457×10^{-4} 2.4251×10^{-3}	3.4834×10^{-17} 1.7498×10^{-6} 6.3084×10^{-17}	5.125
OLBGWO [100]	SDM DDM Photowatt-PWP201	9.86×10^{-4} 9.83×10^{-4} 2.4×10^{-3}	9.86×10^{-4} 9.85×10^{-4} 2.4×10^{-3}	9.86×10^{-4} 9.86×10^{-4} 2.4×10^{-3}	1.4×10^{-8} 1.78×10^{-6} 2.4284×10^{-9}	4.583
CSOOJAYA [114]	SDM DDM Photowatt-PWP201	9.860219×10^{-4} 9.824849×10^{-4} 2.425075×10^{-3}	9.860219×10^{-4} 9.824849×10^{-4} 2.425075×10^{-3}	9.860219×10^{-4} 9.824849×10^{-4} 2.425075×10^{-3}	4.717305×10^{-17} 5.576332×10^{-17} 2.699858×10^{-17}	4.917
DEDIWPSO [85]	SDM DDM Photowatt-PWP201	7.730062×10^{-4} 7.182306×10^{-4} 2.03992×10^{-3}	7.730062×10^{-4} 7.187462×10^{-4} 2.03992×10^{-3}	7.730062×10^{-4} 7.318100×10^{-4} 2.03992×10^{-3}	5.18668×10^{-15} 2.486129×10^{-6} 2.995389×10^{-15}	2.5
EOTLBO [21]	SDM DDM Photowatt-PWP201	$9.86021878 \times 10^{-4}$ $9.82484852 \times 10^{-4}$ $2.42507487 \times 10^{-3}$	$9.86021878 \times 10^{-4}$ $9.84733697 \times 10^{-4}$ $2.42507487 \times 10^{-3}$	$9.86021878 \times 10^{-4}$ $9.89424104 \times 10^{-4}$ $2.42507487 \times 10^{-3}$	$4.12665088 \times 10^{-17}$ $1.69176118 \times 10^{-6}$ $3.61995116 \times 10^{-17}$	4.5
IWOA [123]	SDM DDM Photowatt-PWP201	9.860219×10^{-4} 9.824849×10^{-4} 2.425075×10^{-3}	9.860219×10^{-4} 9.826140×10^{-4} 2.425075×10^{-3}	9.860219×10^{-4} 9.860219×10^{-4} 2.425075×10^{-3}	5.12×10^{-16} 9.86×10^{-5} 2.90×10^{-17}	6.375
TLBOBSA [134]	SDM DDM Photowatt-PWP201	9.86902×10^{-4} 9.8155×10^{-4} 2.42507×10^{-3}	9.8602×10^{-4} 1.1334×10^{-3} 2.42535×10^{-3}	9.8603×10^{-4} 2.2181×10^{-3} 2.43167×10^{-3}	5.64965×10^{-10} 3.0012×10^{-4} 1.21238×10^{-6}	8.292
IGSK [136]	SDM DDM Photowatt-PWP201	9.8602188×10^{-4} 9.8248485×10^{-4} 2.4250749×10^{-3}	9.8602188×10^{-4} 9.8272774×10^{-4} 2.4250749×10^{-3}	9.8602188×10^{-4} 9.8602188×10^{-4} 2.4250749×10^{-3}	$3.5821018 \times 10^{-17}$ 8.9578942×10^{-7} $2.9226647 \times 10^{-17}$	4.333
HSOA [143]	SDM DDM Photowatt-PWP201	9.8602×10^{-4} 9.8376×10^{-4} 2.4251×10^{-3}	1.0479×10^{-3} 1.1175×10^{-3} 2.4251×10^{-3}	1.1683×10^{-3} 1.7642×10^{-3} 2.4253×10^{-3}	5.3832×10^{-5} 1.9107×10^{-4} 4.1556×10^{-8}	9.333
SOS [146]	SDM DDM Photowatt-PWP201	9.8609×10^{-4} 9.8518×10^{-4} 2.4251×10^{-3}	1.0245×10^{-3} 1.0627×10^{-3} 2.4361×10^{-3}	1.1982×10^{-3} 1.3498×10^{-3} 2.5103×10^{-3}	5.2184×10^{-5} 9.6141×10^{-5} 1.7503×10^{-5}	10.083

The variants of metaheuristics that used the SIAE indicators are selected for further comparison in Figure 5, i.e., SOS, HSOA, GSK, TLBOBSA, DE/WOA, ISNMWOA, MCSWOA, IWOA, DMTLBO, PSO-ST, GCPSO, MLJAYA, I-GWO, HDE, DPDE, QILDE, ABC-TRR, and TLABC. Moreover, these methods were generally tested in the SDM, DDM, and Photowatt-PWP201 module. Here, the module only means the Photowatt-PWP201.

- The STD of RMSE reflects the results' robustness, MIN RMSE means the results' accuracy, and other RMSEs denote the range and sharpness of the fluctuations in the results. The SDM, DDM and Photowatt-PWP201 models of DEDIWPSO had the MIN RMSE (7.730062×10^{-4}, 7.182306×10^{-4}, and 2.03992×10^{-3}), mean RMSE (7.730062×10^{-4}, 7.187462×10^{-4}, and 2.03992×10^{-3}), MAX RMSE (7.730062×10^{-4}, 7.3181×10^{-4}, and 2.03992×10^{-3}) and STD (5.18668×10^{-15}, 2.486129×10^{-6}, and 2.995389×10^{-15}). It is followed by IGSK with MIN RMSE (9.8602188×10^{-4}, 9.8248485×10^{-4}, and 2.4250749×10^{-3}), mean RMSE (9.8602188×10^{-4}, 9.8272774×10^{-4}, and 2.4250749×10^{-3}), MAX MRSE (9.8602188×10^{-4}, 9.8602188×10^{-4}, and 2.4250749×10^{-3}) and STD ($3.5821018 \times 10^{-17}$, 8.9578942×10^{-7}, and $2.9226647 \times 10^{-17}$). Then, EOTLBO, OLBGWO, CSOOJAYA, RLDE, ABC-TRR, IWOA, TLBOBSA, HSOA, and SOS followed.
- Figure 4 shows the combined FT ranking for the SDM, DDM, and Photowatt-PWP201. It combines the absolute accuracy of the methods in a wide range of cases. GSK ranks first, followed by MCSWOA, IWOA, GCPSO, QILDE, DE/WOA, DMTLBO, HSOA, MLJAYA, SOS, TLABC, PSO-ST, ABC-TRR, I-GWO, HDE, TLBOBSA, ISNMWOA, and DPDE. GSK, as a new method achieving the highest accuracy, demonstrates the need to explore the performance of new schemes in this issue. It is worth noting that the rankings of the same methods in different PV models may differ, which indicates that different PV models have varied preferences for algorithms.
- TNFES is related to the computational resources consumed, with a lower TNFES representing a lower computational burden. For the SDM and module, ABC-TRR had the fewest TNFES (1000) while other methods basically used a TNFES of 50,000. For the DDM, ABC-TRR had the fewest TNFES (5000), while most of the rest consumed a TNFES of 50,000.

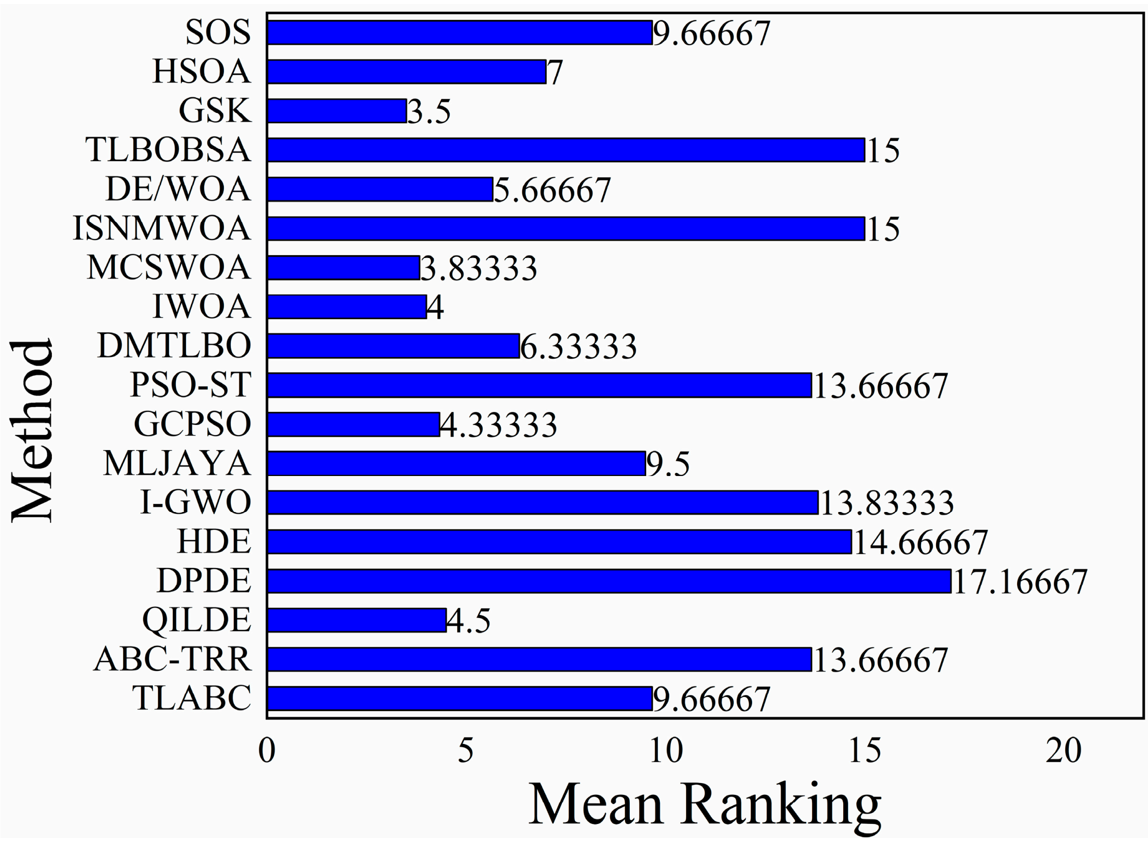

Figure 5. Various methods' Friedman Test.

4.2. Analysis of Temperature and Irradiance Influences

When the irradiance or temperature changes, the current output of the PV cell will also change, and therefore several unknown parameters representing the output characteristics of the PV cell will also change. The GSK algorithm with high accuracy is used in this section to identify the sampled data at different temperatures or irradiances in order to explore their patterns. The data are taken from the KC200GT module in Simulink.

4.2.1. Uniform Irradiance and Temperature

Eight cases under uniform conditions were set up to explore the effects of irradiance and temperature separately. The cases can be divided into five irradiances at 25 °C: 1000, 800, 600, 400, and 200 W/m^2 and four temperatures at 1000 W/m^2: 25, 40, 55, and 70 °C. Their I-V and P-V output characteristics are shown in Figures 6 and 7. In the figures, the output current increases with increasing irradiance, and the maximum power point voltage decreases with increasing temperature.

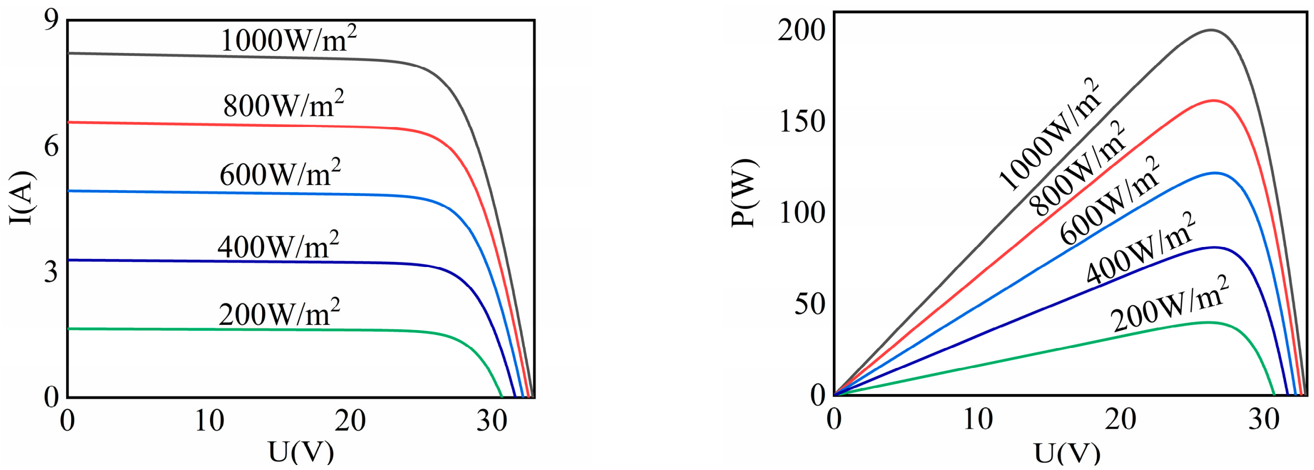

(**a**) (**b**)

Figure 6. Characteristic curves in various irradiance: (**a**) I-V (**b**) P-V.

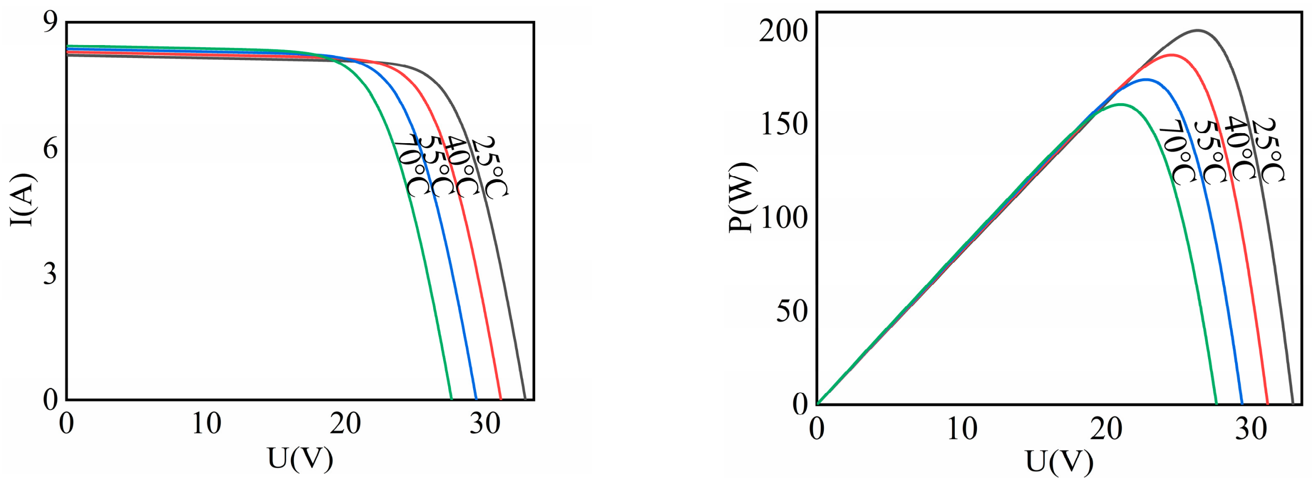

(**a**) (**b**)

Figure 7. Characteristic curves in various temperatures: (**a**) I-V (**b**) P-V.

From the above characteristic plots, it is evident that when environmental factors change, corresponding parameters change accordingly to achieve a high degree of fit to the output curve. The unknown parameters extracted using GSK are illustrated in Table 21. When the irradiance is the variable, I_{ph} increases linearly with increasing irradiance, and R_s decreases in a non-linear fashion with increasing irradiance. When the temperature is the variable, I_{ph} increases weakly with increasing temperature, and I_{ssd} increases in a non-linear manner. Meanwhile, the RMSE increases with decreasing temperature, indicating that the lower the temperature, the lower the identification result's accuracy.

Table 21. Parameters of the KC200GT at different irradiances and temperatures.

Radiation /W/m^2	Temperature /°C	I_{ph}/A	I_{ssd}/μA	n	R_s/Ω	R_{sh}/Ω	RMSE
Variable	Fixed						
1000	25	8.22920506	$2.19226333 \times 10^{-10}$	0.34555194	149.79495733	52.64769156	$2.87908987 \times 10^{-3}$
800	25	6.58249378	$2.57655463 \times 10^{-10}$	0.34314866	190.38069917	52.99842155	$2.40659465 \times 10^{-3}$
600	25	4.93738274	$2.27177693 \times 10^{-10}$	0.34433472	250.19011038	52.72470592	$3.70428705 \times 10^{-3}$
400	25	3.29180014	$1.99109819 \times 10^{-10}$	0.34972198	372.27107651	52.42424407	$1.44743443 \times 10^{-3}$
200	25	1.64555637	$2.50815014 \times 10^{-10}$	0.34381397	769.17560620	52.94945965	$1.23547582 \times 10^{-3}$
Fixed	Variable						
1000	25	8.22811095	$2.49012735 \times 10^{-10}$	0.34410634	152.34953496	52.92528529	$5.10117026 \times 10^{-3}$
1000	40	8.30308470	$2.50259970 \times 10^{-9}$	0.34496529	149.56870789	52.70878667	$4.12556209 \times 10^{-3}$
1000	55	8.37565108	$2.31628311 \times 10^{-8}$	0.34480573	153.53100022	52.79148663	$8.96621362 \times 10^{-3}$
1000	70	8.45187588	$1.62391869 \times 10^{-7}$	0.34518787	146.10502751	52.62434432	$1.10992599 \times 10^{-2}$

Some methods counted in Section 3 simulated PV modules at different irradiances and temperatures. The methods are gathered together, as illustrated in Table 22. The methods' quantity is 22, indicating that the proportion of methods discussing these cases is low and that more consideration needs to be placed on these cases in future research work. Most of the 22 methods discussed irradiance and temperature together, and the cases they used most frequently are SM55, ST40, and KC200GT. Thus, other cases could be added to these three implementations in the future so that further generalizability can be demonstrated.

Table 22. Various methods with different irradiance and temperature experiments.

Method	Case	Radiation	Temperature	Describe
FDB-TLABC [96]	SM55, ST40, KC200GT	√	√	Experiments were designed for five sets of irradiances at 25 °C and three sets of temperature at 1000 W/m^2, with RMSEs consistently lying in the order of 1×10^{-5} in the three modules, much better than L-SHADE, LSHADE-EPSIN, and LSHADE-SPACMA.
IADE [68]	SL80CE-36M	√	√	Four sets of discriminative parameters and minimum RMSEs (0.0115, 0.006, 0.0071, 0.0154) were obtained from experiments fitting PV data for four different sets of environmental parameters at two temperatures and two irradiances in random combinations.

Table 22. *Cont.*

Method	Case	Radiation	Temperature	Describe
DE3P [23]	SM55, RSM50, ST40	√	√	Experiments were carried out with five sets of irradiances at constant temperature and three sets of temperature at constant irradiance, with a maximum RMSE of 0.0148 in the results, which is still an acceptable error.
EJADE [69]	SM55, KC200GT	√	√	The optimal average RMSE was obtained consistently with eight competing algorithms for experiments at different irradiances and temperatures. The RMSEs were of order 1×10^{-4} at 25 °C for 200~800 W/m^2 and 1×10^{-3} for the other experiments.
AGA [64]	-	-	√	A PV cell fitting experiment at different temperatures was designed, and the initial and post-simulation parameter values for the standard case were given.
GWO [98]	-	-	√	Ten sets of experiments at different temperatures (−5 °C~45 °C) were designed and showed an enormous advantage in comparison experiments with MMA, with RMSEs almost of order 1×10^{-3} overall.
OLBGWO [100]	ST40, KC200GT	√	√	The experimental design was the same as that of FDB-TLABC. The ST40 module's RMSEs were at or near the 1×10^{-4} order of magnitude. In the KC200GT module, the RMSEs were at or near the 1×10^{-3} order of magnitude.
EJAYA [111]	SM55, KC200GT	√	√	The experimental design was the same as EJADE. The SM55 experiments' RMSEs were in order 1×10^{-4}, and the other experiments' RMSEs were in order 1×10^{-3}.
MPSO [81]	SM55, ST40, KC200GT	√	√	The experimental design was the same as FDB-TLABC. In the KC200GT, the RMSEs were of order 1×10^{-3}; in the other experiments, the RMSEs were of order 1×10^{-4}.
GCPSO [82]	Sharpe ND-R250A5	√	√	Five experiments with different temperatures and irradiances were designed to obtain high fitting accuracy, with an RMSE of order 1×10^{-3}.
DEDIWPSO [85]	JKM330P	√	√	Experiments were designed for five different irradiances and temperatures, RMSE values were obtained consistently, and all RMSEs were of order 1×10^{-3}.
PSO-ST [87,88]	JKM330P	√	√	The same experimental design as DEDIWPSO, with RMSEs of order 1×10^{-3} and standard deviations of RMSEs on order 1×10^{-17}.
PSOCS [88]	SM55, ST40, KC200GT	√	√	The experimental design was the same as FDB-TLABC, with RMSE concentrated at the order of magnitude 1×10^{-2} and 1×10^{-3}.
EOTLBO [21]	Sharpe ND-R250A5	√	√	The experimental design was the same as GCPSO, with RMSEs concentrated at orders 1×10^{-2} and 1×10^{-3}, and significantly better than the ten comparative algorithms in the text.
MTLBO [119]	SM55, ST40	√	√	The experimental design was the same as FDB-TLABC, whose RMSEs were concentrated on orders 1×10^{-3} and 1×10^{-4} and converged slightly faster than ITLBO.

Table 22. *Cont.*

Method	Case	Radiation	Temperature	Describe
WOA [124]	KC200GT	√	√	The fitting experiments were implemented with SDM, DDM, and TDM. The SDM error was 1.6%, the DDM error was 0.3%, and the TDM error was 0.08%. It indicates that, with sufficient computational resources, TDM > DDM > SDM in terms of accuracy.
ISNMWOA [126]	SM55, ST40, KC200GT	√	√	The experimental design was the same as FDB-TLABC, with the RMSEs concentrated on orders 1×10^{-3} and 1×10^{-4}. It showed that ISNMWOA still has high accuracy at low temperatures and irradiance.
SWOA [125]	SM55, SW255, KC200GT	√	√	Experiments were designed for five irradiances and seven temperatures. The RMSEs were concentrated around 1×10^{-2} for the irradiance experiments and around 1×10^{-3} for the temperature experiments.
DE/WOA [127]	JAM6-60-295W-4BB	√	√	Experiments with five irradiances and four temperatures were implemented. Significantly better RMSEs were consistently achieved compared to seven competing algorithms, and all results were concentrated around 1×10^{-5}.
HPSODOX [47]	-	\	√	Seven sets of experiments from −5 to 25 °C were designed. Of these, the RMSEs were located in order 1×10^{-9} at 25 °C and in order 1×10^{-8} at different temperatures.
TLBOBSA [134]	SM55, KC200GT	√	√	The experimental design was the same as EJADE. The experimental results were similar to EJAYA and slightly worse overall.
IGSK [136]	SM55, ST40	√	√	The experimental design was the same as MTLBO, with 11 RMSEs at the 1×10^{-4} order of magnitude and 6 RMSEs at the 1×10^{-3} order of magnitude in 17 experiments.

The "√" means that there are temperature or irradiance experiments in the literature.

4.2.2. Partial Shade Conditions

Four groups of KC200GTs were connected in series to obtain the multi-peak curve exhibited by the output of the PV power system when partially shaded (PSC). Four sets of comparison tests were designed: standard case (STC: 4 × 1000 W/m^2), type I partial shading (PSC-1: 1000, 800, 400, 400 W/m^2), type II partial shading (PSC-2: 800, 600, 400, 200 W/m^2), and type III partial shading (PSC-3: 800, 600, 400, 400 W/m^2). The output characteristics are shown in Figure 8. In the figure, STC has a single peak, PSC-1 and PSC-3 have three peaks, and PSC-2 has four. Additionally, STC has only one irradiance, PSC-1 and PSC-3 have three irradiances, and PSC-2 has four irradiances. Therefore, the PV's peaks are related to the irradiance types on the series-connected PV modules.

The mathematical models developed in Section 2 cannot generate multiple inflection points. Thus, the characteristic curve of the PSC fitted using these mathematical models will still have only one inflection point, and the accuracy of the fit will be very low. It is reflected in a large minimum RMSE. The extracted parameters are shown in Table 23, and it is clear that the RMSE at STC is much lower than that at PSC. Although the corresponding mathematical model was developed by Chellaswamy et al. [147], it requires human judgment and input of the number of modules to be shaded, which is difficult to achieve in reality. Therefore, more mathematical models need to be developed in future work to improve the accuracy of the parameters of the extracted PSCs. It is important to note that, due to the presence of parallel diodes in the system, the PV modules are in an idle state when the output current of the system is more significant than its photogenerated current.

The mathematical models developed to simulate the output characteristics of the PSC must take this critical point into account.

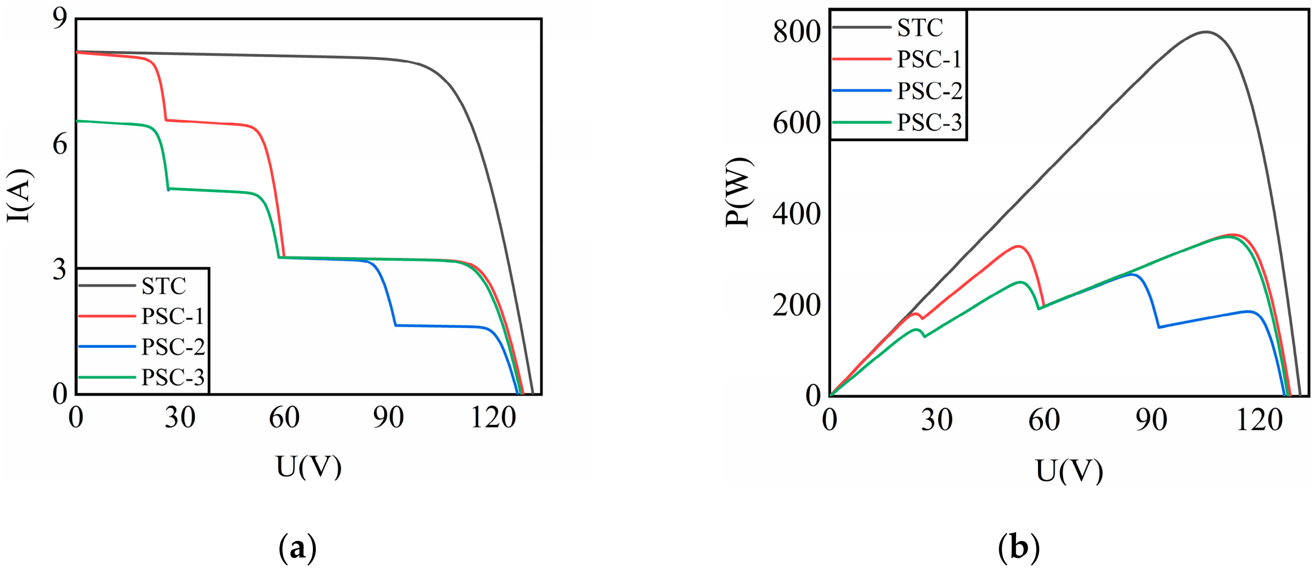

Figure 8. Characteristic curves in partial shade conditions: (**a**) I-V (**b**) P-V.

Table 23. Parameters of the KC200GT at partial shade conditions.

Case	I_{ph}/A	I_{ssd}/μA	n	R_s/Ω	R_{sh}/Ω	RMSE
STC	8.22879884	$2.32498946 \times 10^{-10}$	1.37930864×10^{0}	602.77198763	211.10041272	$1.31085496 \times 10^{-6}$
PSC-1	8.40661915	$3.20394383 \times 10^{-15}$	$1.62587931 \times 10^{-16}$	18.94997935	149.17780560	$6.96889061 \times 10^{-1}$
PSC-2	6.93947342	$1.16187272 \times 10^{-14}$	$2.40441463 \times 10^{-16}$	20.81282985	155.76285151	$3.71532656 \times 10^{-1}$
PSC-3	6.52880635	$5.19579219 \times 10^{-12}$	$1.10570546 \times 10^{-14}$	28.77275463	188.22179994	$4.55796025 \times 10^{-1}$

4.3. Analysis of Modified Diode Models' Works

The MSDM, MDDM, and MTDM all consider the quasi-neutral zone's losses. It is reflected in the circuit diagram by selecting a diode branch and adding a series resistor R_{sm}. The improved model adds an unknown parameter compared to the pre-improved model. Their circuit diagram is shown in Figure 9.

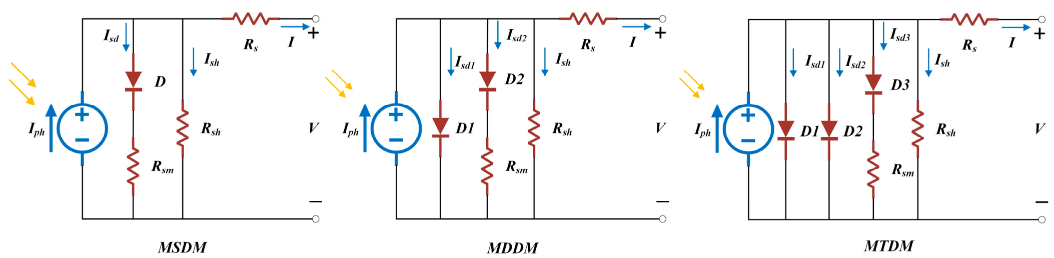

Figure 9. Modified diode models' circuits.

Their output current changes to [48,49]:

$$I = I_{ph} - \frac{V + IR_s}{R_{sh}} - \sum_{j=1 \to (nD-1)} I_{ssdj}\left[\exp\left(\frac{q(V+IR_s)}{n_j kT}\right) - 1\right] - I_{ssdnD}\left[\exp\left(\frac{q(V+IR_s - I_{sdnD}R_{sm})}{n_{nD}kT}\right) - 1\right] \quad (14)$$

where nD represents the number of diodes in the cell model.

In this subsection, two papers from the last three years are chosen to present the results of metaheuristic approaches to solving the above models. Ramadan et al. [48] improved the Bald Eagle Search algorithm (IBES), employing decay equations to achieve adaptive learning factors. Abdelminaam et al. [49] pioneered the use of Turbulent Flow Optimization of Water (TFWO) for the parameter extraction of PV cells with a new objective function (PE5DSSE). Their extraction results are illustrated in Table 24.

Table 24. Results of the modified diode models.

Parameter	IBES MSDM	TFWO MSDM	IBES MDDM	TFWO MDDM	IBES MTDM	TFWO MTDM
I_{ph}/A	0.760713	0.760774525	0.760494	0.760783023	0.760473235	0.760780283
R_s/Ω	0.032091	0.037372671	0.015196	0.036835645	0.013865736	0.036749141
R_{sh}/Ω	54.30519	53.7186078	54.05261	55.8909553	55.47156858	55.52672891
R_{sm}/Ω	0.00352	0.5	0.02792	0.01025276	0.027870684	0.5
$I_{ssd1}/\mu\mathrm{A}$	3.71×10^{-7}	3.23×10^{-7}	1.00×10^{-10}	9.17×10^{-7}	1.00×10^{-10}	7.63×10^{-7}
$I_{ssd2}/\mu\mathrm{A}$	-	-	6.69×10^{-7}	2.07×10^{-7}	7.52×10^{-7}	2.47×10^{-9}
$I_{ssd3}/\mu\mathrm{A}$	-	-	-	-	1.00×10^{-10}	2.24×10^{-7}
n_1	1.4835	1.48118376	1.00	1.999992291	1.133059042	2
n_2	-	-	1.525277	1.443600817	1.537322148	2
n_3	-	-	-	-	1.004574508	1.450312839
PE5DSSE	-	2.5278×10^{-5}	-	2.51×10^{-5}	-	2.509×10^{-5}
MIN RMSE	9.61×10^{-4}	-	7.49×10^{-4}	-	7.39055×10^{-4}	-
Mean RMSE	1.507×10^{-3}	-	1.201×10^{-3}	-	7.64×10^{-4}	-
MAX RMSE	2.847×10^{-3}	-	3.378×10^{-3}	-	7.81×10^{-4}	-
STD of RMSE	7.61×10^{-4}	-	8.95×10^{-4}	-	2.21×10^{-5}	-

In Table 24, for MSDM, the parameter that differs most between IBES and TFWO is R_{sm}. For MDDM, IBES and TFWO are similar in I_{ph} and R_{sh}, and the other parameters differ more. For MTDM, IBES and TFWO are almost identical in I_{ph} and R_{sh}, and the other parameters differ more. As they use different objective functions, it is impossible to compare the accuracy of the two.

In IBES, the MIN RMSE is 9.88×10^{-4} for TDM and 9.86×10^{-4} for SDM and DDM. In TFWO, the PE5DSSE is 2.5278×10^{-5} for SDM, 2.51×10^{-5} for DDM and 2.51×10^{-5} for TDM. It indicates that the addition of Rsh did improve the accuracy by a small margin. Therefore, applying MSDM, MDDM, MTDM, and the PV module models constructed from them to future studies will be an effective way to improve the accuracy further.

4.4. Analysis of Dynamic Models' Works

The above results are for static models. This subsection starts with several representative metaheuristics for solving dynamic models to analyze their parameter extraction results.

Yousri et al. [52] developed CHCLPSO by combining heterogeneous integrated learning PSO with chaotic optimization techniques. HROA was developed along similar lines to CHCLPSO, a hybrid of the chaotic mapping mechanism with the Rao_1 algorithm by Wang et al. [53]. Elaziz et al. [51] developed EMPA by an effective combination of DE and the Marine Predator algorithm.

For the results of the dynamic model, CHCLPSO provides parameters of $R_C = 7.3149\ \Omega$, $C = 3.81307 \times 10^{-7}$ F, and $L = 7.3251 \times 10^{-6}$ H. EMPA provides parameters of $R_C = 7.315\ \Omega$, $C = 3.1831 \times 10^{-7}$ F, and $L = 7.3251 \times 10^{-6}$ H. Their difference is insignificant, indicating that both methods have similar solving power. The MIN and Mean RMSEs for CHCLPSO are 8.45045×10^{-3}, and the STD is 1.13566×10^{-12}. The MIN, Mean, and MAX RMSEs for HROA are 6.709393×10^{-3}, and the STD is 5.209153×10^{-18}. The Mean RMSE for EMPA makes it clear that HROA has the best accuracy and robustness, followed by EMPA and CHCLPSO. However, CHCLPSO is at the same level of accuracy as EMPA, and both have a minor STD. This indicates that EMPA and CHCLPSO have converged early, and their further improvement needs to start from exploration. For HROA, it achieves the optimal

RMSE value, but 6.709393 $\times 10^{-3}$ is still a significant error and there is room for further optimization of the accuracy of the solution.

It is worth mentioning that the model of dynamics is suitable for grid-connected operation. However, there has been little research related to it since its introduction, and especially little research on metaheuristic methods to optimize the dynamic model. Therefore, it has broad application and research prospects and is a crucial research direction for the future.

4.5. Whole Analysis

Pursuant to scholarly opinion and statistical results, Table 25 analyses the positive and negative properties of various metaheuristics. They can help beginners to understand cutting-edge research.

Table 25. Various methods' positive and negative properties.

Type	Positive	Negative
GAs	• Using probabilistic mutation techniques • Fast handling of non-linear problems [63] • Easily contribute to the convergence and accuracy of other methods [65]	• Reliance on the initialized populations' quality • Lower accuracy of solution than advanced methods
DEs	• Simple and precise implementation • Steady and fast • Extensible, with many variants • Employing adequate parameter tweaking mechanisms ensures an overall improvement in the algorithm's capabilities in specific problems [41,68,76]	• The parameters' decision shapes the results • Computing resources are underutilized
PSOs	• Straightforward code • Fast merit search • Low fluctuant solution and efficient • Supports parallel operation for faster and greater accuracy [86] • For the problems in this paper, PSO secured quality solutions [82,83]	• Excessive parameters and empirical reliance • Converge prematurely • Prone to converge to local optimum in multi-peaked issues
ABCs	• Superb exploration [92] • Rapid convergence [89] • Simplicity implementation [93] • Fits PV characteristic curves more accurately than PSO [95] • Premium performance in combination with alternative methods [91,94]	• Weak exploitation • Parameters and performance are strongly correlated
GWOs	• A few parameters • Flexibility and simplicity • Well-aligned exploration and exploitation [97] • Tackling PV parameter estimation issues with small errors [98]	• Poor handling issues with numerous variables • Exploitation requires reinforcement [100]

Table 25. *Cont.*

Type	Positive	Negative
JAYAs	• No parameters • Efficient and succinct • Adaptive control factor optimizes accuracy and stability [104,107] • Mixing different methods of consideration facilitates performance improvement [106,111]	• Weak exploration [108] • Pseudo-random operators restricted pervasiveness • Performance degradation in multi-dimensional issues [103]
TLBOs	• No parameters • Universal in optimization issues • Competitive in large scale issues [115] • Diverse variants enhance behavior when employed for specific problems [118,120]	• Slow convergence [116] • Mandatory structures squandering resources [21] • Inadequate balance of exploration and exploitation [117,118]
WOAs	• A few parameters • Simple structure • Intense exploitation competency [123] • Variant with outstanding solutions quality [125,126]	• Premature convergence [18] • Poor in convergence and precision • Performance degradation in complex issues
GSKs	• Intense exploration competency [4] • Competitive in multidimensional issues • Fits PV characteristic curve accurately [136]	• Excessive parameters • Weak exploitation
SDOs	• A few parameters • Simple structure • Well-balanced exploration and exploitation [137]	• Poor in convergence • Needs improvement in solution quality [39]
HHOs	• Fewer mechanisms, simpler calculations [148] • Fast convergence [135] • Suitable for multimodal scenarios [55]	• Excessive parameters • Premature convergence
TGAs	• Simple structure • High accuracy of identification results • Highly competitive [138]	• Excessive parameters • Slow convergence • Excessive consumption of computational resources
SOSs	• No parameters • Simple structure • Superb exploration [146]	• Weak exploitation • Excessive resources consumption
FPOAs	• Fewer parameters • Easy to implement • Simple structure • More accurate than PSO and DE [145]	• Premature convergence • Slow convergence

For the different applied metaheuristics, we find the following challenges.

1. The promotion of GA has been rare in recent years, and accuracy is supposed to be enhanced.
2. DE's convergence rate and PSO's accuracy could improve.
3. ABC is weakly exploited and significant in parameter settings.
4. GWO and WOA have few parameters and struggle with multi-dimensional issues.
5. JAYA and TLBO's promotions are flawed in accuracy.
6. Hybrid approaches may complicate the implementation and introduce additional parameters.

7. New approaches are not sufficiently balanced for specific issues. For example, GSK, SDO, TGA, and SOS are under-exploited, and HHO and FPOA are under-explored.

The challenges above are all tailored to specific metaheuristics. Moreover, several additional challenges remain for the parameter extraction problem.

1. TNFES is a sign of computational resources, yet its value is almost pitched at 50,000. Reducing TNFES without compromising accuracy is imperative.
2. More diodes in the cell model may increase the extraction accuracy. Recently, a four diode model was proposed [47] and the results showed good fitting effect. However, more diodes also indicate more parameters that need to be extracted and solutions are also more intractable. Hence, selecting a suitable PV model for an algorithm is challenging.
3. Some of the literature used too few PV cases to demonstrate metaheuristics' generalizability.
4. Metaheuristics' effectiveness is devoid of practical engineering applications.
5. More and exact measured data means more accurate extraction results, but obtaining sufficient high-precision measurements is challenging and costly.
6. In engineering, running time is pivotal. Hence, cutting running times is a challenge.
7. Multiple matrices are imperative to signal the competitiveness of metaheuristic results, yet some of the literature adopted few matrices for comparison.

4.6. Research Prospects

The previous section summarizes the challenges in studies, and this section suggests some research directions. They are an essential reference for researchers in developing their plans.

For specific metaheuristics:

1. Exploration techniques such as chaotic mapping and second-order oscillation mechanisms can be considered to incorporate into GA. They are envisaged to augment accuracy and robustness.
2. DE might be combined with exploitation-based metaheuristics, such as the Search Backtracking Algorithm, or with search mechanisms that accelerate the convergence. PSO demands more diversity-raising search mechanisms such as trust region reflection, taboo search, and fitness distance balance. Additionally, studies on adapting their parameters are well-tried.
3. ABC considers introducing neighborhood search and adaptive mechanisms to speed up the convergence.
4. For GWO and WOA, adaptive operators could be inserted to improve applicability in the face of high-dimensional issues.
5. JAYA and TLBO could borrow the exploration-type mechanisms in CSOOJAYA, MTLBO, and EBLSHADE to improve the overall performance.
6. Hybrid methods can identify contributing components through component analysis and remove unimportant components to alleviate implementation redundancy.
7. New methods can adopt adaptive learning, neighborhood search, chaotic mapping, and algorithmic blending techniques to enhance their behavior.

Regardless of the specific techniques, any approach to raise the metaheuristics is to employ complementary improvements to balance exploration and exploitation and, ultimately, fit to the studied issue.

In addition to research directions for metaheuristics, some potential directions for application scenarios include the following areas:

1. For the parameter extraction, diminishing computational resources' consumption is at stake. Reducing TNFES while maintaining the same accuracy by introducing different techniques, i.e., local search and reinforcement learning, is a direction worthy of further research.

2. Some methods are feasible for low-dimensional issues, and some deliver better performance for high-dimensional issues. Meanwhile, the selection of MSDM, MDDM, MTDM, and FDM with 6, 8, 10, and 11 unknown parameters to be included in the cell model is a future research direction for further performance improvement. Hence, it would be interesting to pick the right algorithm improvement to render PV models with desirable accuracy.
3. For the issue of too few employed cases, more cases are considered in future research to reveal the methods' generalizability. Examples include cases at different temperatures and irradiances and cases in partial shade.
4. The real-time extraction of PV models' parameters at different operating conditions is highly suggested. It is excellent work to accurately model the dynamics of photovoltaics for practical engineering problems.
5. Faced with the problem of little measured data, inserting deep learning techniques such as neural networks to eliminate erroneous data and expand the amount of data for metaheuristic methods is an effective way to facilitate the extraction accuracy.
6. The graphical processing unit (GPU) allows different solutions to be updated simultaneously to raise the efficiency. Thus, metaheuristic methods' speed improvements can be geared toward direct runtime reductions through GPU-like devices.
7. More performance evaluation indicators can demonstrate metaheuristic methods' overall effectiveness more comprehensively. Therefore, introducing more multifaceted indicators is necessary to enhance persuasiveness.

5. Conclusions

PV generation is playing a more significant role in the future energy landscape. Meanwhile, accurate PV models can support the PV systems' accurate assessment, efficiency improvement, fault analysis, and simulation. Thus, this paper reviewed different metaheuristics employed in the PV model parameters extraction. In our work, (a) the PV models and problem formulations were explained; (b) different metaheuristics and their developments and applications were summarized; (c) the algorithmic parameter settings, various evaluation indicators, independent running numbers, and computational resources (TNFES) were assembled; (d) the final results of various algorithms were compared, and especially RMSE and SIAE were ranked; (e) the unknown parameters and RMSE variation patterns in different environments were analyzed; and (f) a comprehensive analysis of the challenges encountered by metaheuristics in solving the studied issue was presented, and some ideas for future research were outlined.

This study can assist beginners in gaining an introductory and systematic perspective on the issue. It may also provide a reference direction for further research when unfamiliar researchers understand the application of metaheuristics to this engineering problem.

Author Contributions: Conceptualization, Z.G. and G.X.; methodology, G.X.; formal analysis, G.X. and X.F.; writing—original draft preparation, Z.G.; writing—review and editing, G.X. and X.F.; supervision, G.X. All authors have read and agreed to the published version of the manuscript.

Funding: This research was funded by the National Natural Science Foundation of China, grant number 52167007, the Natural Science Foundation of Guizhou Province, grant number QiankeheBasic-ZK [2022] General121, the Innovation Foundation of Guizhou University Institute of Engineering Investigation and Design Co., Ltd., grant number GuiDaKanCha [2022]03, and the Modern Power System and Its Digital Technology Engineering Research Center, grant number QianJiaoJi [2022]043.

Institutional Review Board Statement: Not applicable.

Informed Consent Statement: Not applicable.

Data Availability Statement: Not applicable.

Conflicts of Interest: The authors declare no conflict of interest.

References

1. Li, Y.; Chiu, Y.H.; Lin, T.Y. Research on New and Traditional Energy Sources in OECD Countries. *Int. J. Environ. Res. Public Health* **2019**, *16*, 1122. [CrossRef]
2. Ridha, H.M.; Heidari, A.A.; Wang, M.; Chen, H. Boosted mutation-based Harris hawks optimizer for parameters identification of single-diode solar cell models. *Energy Convers. Manag.* **2020**, *209*, 112660. [CrossRef]
3. You, V.; Kakinaka, M. Modern and traditional renewable energy sources and CO(2) emissions in emerging countries. *Environ. Sci. Pollut. Res.* **2022**, *29*, 17695–17708. [CrossRef] [PubMed]
4. Xiong, G.; Li, L.; Mohamed, A.W.; Yuan, X.; Zhang, J. A new method for parameter extraction of solar photovoltaic models using gaining–sharing knowledge based algorithm. *Energy Rep.* **2021**, *7*, 3286–3301. [CrossRef]
5. Lin, S.; Zhang, C.; Ding, L.; Zhang, J.; Liu, X.; Chen, G.; Wang, S.; Chai, J. Accurate Recognition of Building Rooftops and Assessment of Long-Term Carbon Emission Reduction from Rooftop Solar Photovoltaic Systems Fusing GF-2 and Multi-Source Data. *Remote Sens.* **2022**, *14*, 3144. [CrossRef]
6. Dixit, S. Solar technologies and their implementations: A review. *Mater. Today Proc.* **2020**, *28*, 2137–2148. [CrossRef]
7. Kant Bhatia, S.; Palai, A.K.; Kumar, A.; Kant Bhatia, R.; Kumar Patel, A.; Kumar Thakur, V.; Yang, Y.H. Trends in renewable energy production employing biomass-based biochar. *Bioresour. Technol.* **2021**, *340*, 125644. [CrossRef]
8. Qazi, A.; Hussain, F.; Rahim, N.A.B.D.; Hardaker, G.; Alghazzawi, D.; Shaban, K.; Haruna, K. Towards Sustainable Energy: A Systematic Review of Renewable Energy Sources, Technologies, and Public Opinions. *IEEE Access* **2019**, *7*, 63837–63851. [CrossRef]
9. Rojas, D.; Rivera, M.; Wheeler, P. Basic Principles of Solar Energy. In Proceedings of the 2021 IEEE CHILEAN Conference on Electrical, Electronics Engineering, Information and Communication Technologies (CHILECON), Valparaíso, Chile, 6–9 December 2021; pp. 1–6.
10. Saidur, R.; BoroumandJazi, G.; Mekhlif, S.; Jameel, M. Exergy analysis of solar energy applications. *Renew. Sustain. Energy Rev.* **2012**, *16*, 350–356. [CrossRef]
11. Zheng, Y.; Weng, Q. Modeling the Effect of Green Roof Systems and Photovoltaic Panels for Building Energy Savings to Mitigate Climate Change. *Remote Sens.* **2020**, *12*, 2402. [CrossRef]
12. Chen, D.-Y.; Peng, L.; Zhang, W.-Y.; Wang, Y.-D.; Yang, L.-N. Research on Self-Supervised Building Information Extraction with High-Resolution Remote Sensing Images for Photovoltaic Potential Evaluation. *Remote Sens.* **2022**, *14*, 5350. [CrossRef]
13. Humada, A.M.; Darweesh, S.Y.; Mohammed, K.G.; Kamil, M.; Mohammed, S.F.; Kasim, N.K.; Tahseen, T.A.; Awad, O.I.; Mekhilef, S. Modeling of PV system and parameter extraction based on experimental data: Review and investigation. *Sol. Energy* **2020**, *199*, 742–760. [CrossRef]
14. Kumari, P.A.; Geethanjali, P. Parameter estimation for photovoltaic system under normal and partial shading conditions: A survey. *Renew. Sustain. Energy Rev.* **2018**, *84*, 1–11. [CrossRef]
15. Pillai, D.S.; Rajasekar, N. Metaheuristic algorithms for PV parameter identification: A comprehensive review with an application to threshold setting for fault detection in PV systems. *Renew. Sustain. Energy Rev.* **2018**, *82*, 3503–3525. [CrossRef]
16. Humada, A.M.; Hojabri, M.; Mekhilef, S.; Hamada, H.M. Solar cell parameters extraction based on single and double-diode models: A review. *Renew. Sustain. Energy Rev.* **2016**, *56*, 494–509. [CrossRef]
17. Selem, S.I.; El-Fergany, A.A.; Hasanien, H.M. Artificial electric field algorithm to extract nine parameters of triple-diode photovoltaic model. *Int. J. Energy Res.* **2020**, *45*, 590–604. [CrossRef]
18. Xiong, G.; Zhang, J.; Shi, D.; Zhu, L.; Yuan, X.; Yao, G. Modified Search Strategies Assisted Crossover Whale Optimization Algorithm with Selection Operator for Parameter Extraction of Solar Photovoltaic Models. *Remote Sens.* **2019**, *11*, 2795. [CrossRef]
19. Abbassi, R.; Abbassi, A.; Jemli, M.; Chebbi, S. Identification of unknown parameters of solar cell models: A comprehensive overview of available approaches. *Renew. Sustain. Energy Rev.* **2018**, *90*, 453–474. [CrossRef]
20. Li, S.; Gong, W.; Gu, Q. A comprehensive survey on meta-heuristic algorithms for parameter extraction of photovoltaic models. *Renew. Sustain. Energy Rev.* **2021**, *141*, 110828. [CrossRef]
21. Xiong, G.; Zhang, J.; Shi, D.; Zhu, L.; Yuan, X. Parameter extraction of solar photovoltaic models with an either-or teaching learning based algorithm. *Energy Convers. Manag.* **2020**, *224*, 113395. [CrossRef]
22. Ibrahim, H.; Anani, N. Evaluation of Analytical Methods for Parameter Extraction of PV modules. *Energy Procedia* **2017**, *134*, 69–78. [CrossRef]
23. Chin, V.J.; Salam, Z. A New Three-point-based Approach for the Parameter Extraction of Photovoltaic Cells. *Appl. Energy* **2019**, *237*, 519–533.
24. Abbassi, A.; Gammoudi, R.; Ali Dami, M.; Hasnaoui, O.; Jemli, M. An improved single-diode model parameters extraction at different operating conditions with a view to modeling a photovoltaic generator: A comparative study. *Sol. Energy* **2017**, *155*, 478–489. [CrossRef]
25. Nguyen, H.; Nguyen, D.; Ngo, A.P.; Thomas, C. Solar PV Modeling with Lambert W Function: An Exponential Cone Programming Approach. In Proceedings of the 2022 IEEE Kansas Power and Energy Conference (KPEC), Manhattan, KS, USA, 25–26 April 2022; pp. 1–5.
26. Sharadga, H.; Hajimirza, S.; Cari, E.P.T. A Fast and Accurate Single-Diode Model for Photovoltaic Design. *IEEE J. Emerg. Sel. Top. Power Electron.* **2021**, *9*, 3030–3043. [CrossRef]

27. Tina, G.M.; Ventura, C.; Ferlito, S.; De Vito, S. A State-of-Art-Review on Machine-Learning Based Methods for PV. *Appl. Sci.* **2021**, *11*, 7550. [CrossRef]
28. Eslami, M.; Akbari, E.; Seyed Sadr, S.T.; Ibrahim, B.F. A novel hybrid algorithm based on rat swarm optimization and pattern search for parameter extraction of solar photovoltaic models. *Energy Sci. Eng.* **2022**, *10*, 2689–2713. [CrossRef]
29. Huang, T.; Zhang, C.; Ouyang, H.; Luo, G.; Li, S.; Zou, D. Parameter identification for photovoltaic models using an improved learning search algorithm. *IEEE Access* **2020**, *8*, 116292–116309. [CrossRef]
30. Rizk-Allah, R.M.; Hassanien, A.E. Locomotion-based Hybrid Salp Swarm Algorithm for Estimation of Fuzzy Representation-based Photovoltaic Modules. *J. Mod. Power Syst. Clean Energy* **2021**, *9*, 384–394. [CrossRef]
31. Yu, K.; Liang, J.J.; Qu, B.Y.; Cheng, Z.; Wang, H. Multiple learning backtracking search algorithm for estimating parameters of photovoltaic models. *Appl. Energy* **2018**, *226*, 408–422. [CrossRef]
32. Oliva, D.; Elaziz, M.A.; Elsheikh, A.H.; Ewees, A.A. A review on meta-heuristics methods for estimating parameters of solar cells. *J. Power Sources* **2019**, *435*, 126683. [CrossRef]
33. Venkateswari, R.; Rajasekar, N. Review on parameter estimation techniques of solar photovoltaic systems. *Int. Trans. Electr. Energy Syst.* **2021**, *31*, e13113. [CrossRef]
34. Chen, Z.; Lin, W.; Wu, L.; Long, C.; Peijie, L.; Cheng, S. A capacitor based fast I-V characteristics tester for photovoltaic arrays. *Energy Procedia* **2018**, *145*, 381–387. [CrossRef]
35. Toledo, F.J.; Blanes, J.M. Geometric properties of the single-diode photovoltaic model and a new very simple method for parameters extraction. *Renew. Energy* **2014**, *72*, 125–133. [CrossRef]
36. Li, D.; Yang, B.; Li, L.; Li, Q.; Deng, J.; Guo, C. Recent Photovoltaic Cell Parameter Identification Approaches: A Critical Note. *Front. Energy Res.* **2022**, *10*, 902749. [CrossRef]
37. Younis, A.; Bakhit, A.; Onsa, M.; Hashim, M. A comprehensive and critical review of bio-inspired metaheuristic frameworks for extracting parameters of solar cell single and double diode models. *Energy Rep.* **2022**, *8*, 7085–7106. [CrossRef]
38. Sun, L.; Wang, J.; Tang, L. A Powerful Bio-Inspired Optimization Algorithm Based PV Cells Diode Models Parameter Estimation. *Front. Energy Res.* **2021**, *9*, 675925. [CrossRef]
39. Shaheen, A.M.; El-Seheimy, R.A.; Xiong, G.; Elattar, E.; Ginidi, A.R. Parameter identification of solar photovoltaic cell and module models via supply demand optimizer. *Ain Shams Eng. J.* **2022**, *13*, 101705. [CrossRef]
40. Qais, M.H.; Hasanien, H.M.; Alghuwainem, S. Parameters extraction of three-diode photovoltaic model using computation and Harris Hawks optimization. *Energy* **2020**, *195*, 117040. [CrossRef]
41. Hu, Z.; Gong, W.; Li, S. Reinforcement learning-based differential evolution for parameters extraction of photovoltaic models. *Energy Rep.* **2021**, *7*, 916–928. [CrossRef]
42. Jordehi, A.R. Parameter estimation of solar photovoltaic (PV) cells: A review. *Renew. Sustain. Energy Rev.* **2016**, *61*, 354–371. [CrossRef]
43. Nishioka, K.; Sakitani, N.; Uraoka, Y.; Fuyuki, T. Analysis of multicrystalline silicon solar cells by modified 3-diode equivalent circuit model taking leakage current through periphery into consideration. *Sol. Energy Mater. Sol. Cells* **2007**, *91*, 1222–1227. [CrossRef]
44. Suskis, P.; Galkin, I. Enhanced Photovoltaic Panel Model for MATLAB-Simulink Environment Considering Solar Cell Junction Capacitance. In Proceedings of the 2013 39th Annual Conference of the IEEE Industrial Electronics Society (IECON), Vienna, Austria, 10–13 November 2013; pp. 1613–1618.
45. Soon, J.J.; Low, K.-S. Optimizing Photovoltaic Model for Different Cell Technologies Using a Generalized Multidimension Diode Model. *IEEE Trans. Ind. Electron.* **2015**, *62*, 6371–6380. [CrossRef]
46. Rawa, M.; Calasan, M.; Abusorrah, A.; Alhussainy, A.A.; Al-Turki, Y.; Ali, Z.M.; Sindi, H.; Mekhilef, S.; Aleem, S.H.E.A.; Bassi, H. Single Diode Solar Cells—Improved Model and Exact Current–Voltage Analytical Solution Based on Lambert's W Function. *Sensors* **2022**, *22*, 4173. [CrossRef] [PubMed]
47. Singh, B.; Singla, M.K.; Nijhawan, P. Parameter estimation of four diode solar photovoltaic cell using hybrid algorithm. *Energy Sources Part A Recovery Util. Environ. Eff.* **2022**, *44*, 4597–4613. [CrossRef]
48. Ramadan, A.; Kamel, S.; Hassan, M.H.; Khurshaid, T.; Rahmann, C. An Improved Bald Eagle Search Algorithm for Parameter Estimation of Different Photovoltaic Models. *Processes* **2021**, *9*, 1127. [CrossRef]
49. Abdelminaam, D.S.; Said, M.; Houssein, E.H. Turbulent Flow of Water-Based Optimization Using New Objective Function for Parameter Extraction of Six Photovoltaic Models. *IEEE Access* **2021**, *9*, 35382–35398. [CrossRef]
50. Di Piazza, M.C.; Luna, M.; Vitale, G. Dynamic PV Model Parameter Identification by Least-Squares Regression. *IEEE J. Photovolt.* **2013**, *3*, 799–806. [CrossRef]
51. Abd Elaziz, M.; Thanikanti, S.B.; Ibrahim, I.A.; Lu, S.; Nastasi, B.; Alotaibi, M.A.; Hossain, M.A.; Yousri, D. Enhanced Marine Predators Algorithm for identifying static and dynamic Photovoltaic models parameters. *Energy Convers. Manag.* **2021**, *236*, 113971. [CrossRef]
52. Yousri, D.; Allam, D.; Eteiba, M.B.; Suganthan, P.N. Static and dynamic photovoltaic models' parameters identification using Chaotic Heterogeneous Comprehensive Learning Particle Swarm Optimizer variants. *Energy Convers. Manag.* **2019**, *182*, 546–563. [CrossRef]
53. Wang, S.; Yu, Y.; Hu, W. Static and dynamic solar photovoltaic models' parameters estimation using hybrid Rao optimization algorithm. *J. Clean. Prod.* **2021**, *315*, 128080. [CrossRef]

54. Ginidi, A.R.; Shaheen, A.M.; El-Sehiemy, R.A.; Elattar, E. Supply demand optimization algorithm for parameter extraction of various solar cell models. *Energy Rep.* **2021**, *7*, 5772–5794. [CrossRef]
55. Chen, H.; Jiao, S.; Wang, M.; Heidari, A.A.; Zhao, X. Parameters identification of photovoltaic cells and modules using diversification-enriched Harris hawks optimization with chaotic drifts. *J. Clean. Prod.* **2020**, *244*, 118778. [CrossRef]
56. Song, S.; Wang, P.; Heidari, A.A.; Zhao, X.; Chen, H. Adaptive Harris hawks optimization with persistent trigonometric differences for photovoltaic model parameter extraction. *Eng. Appl. Artif. Intell.* **2022**, *109*, 104608. [CrossRef]
57. Ridha, H.M.; Hizam, H.; Mirjalili, S.; Othman, M.L.; Ya'acob, M.E.; Ahmadipour, M.; Ismaeel, N.Q. On the problem formulation for parameter extraction of the photovoltaic model: Novel integration of hybrid evolutionary algorithm and Levenberg Marquardt based on adaptive damping parameter formula. *Energy Convers. Manag.* **2022**, *256*, 115403. [CrossRef]
58. Mohammed Ridha, H.; Hizam, H.; Mirjalili, S.; Lutfi Othman, M.; Effendy Ya'acob, M.; Ahmadipour, M. Novel parameter extraction for Single, Double, and three diodes photovoltaic models based on robust adaptive arithmetic optimization algorithm and adaptive damping method of Berndt-Hall-Hall-Hausman. *Sol. Energy* **2022**, *243*, 35–61. [CrossRef]
59. Xiong, G.; Zhang, J.; Shi, D.; Zhu, L.; Yuan, X.; Tan, Z. Winner-leading competitive swarm optimizer with dynamic Gaussian mutation for parameter extraction of solar photovoltaic models. *Energy Convers. Manag.* **2020**, *206*, 112450. [CrossRef]
60. Ortiz-Conde, A.; Trejo, O.; Garcia-Sanchez, F.J. Direct Extraction of Solar Cell Model Parameters Using Optimization Methods. In Proceedings of the 2021 IEEE Latin America Electron Devices Conference (LAEDC), Mexico, Mexico, 19–21 April 2021; pp. 1–6.
61. Biswas, P.P.; Suganthan, P.N.; Wu, G.; Amaratunga, G.A.J. Parameter estimation of solar cells using datasheet information with the application of an adaptive differential evolution algorithm. *Renew. Energy* **2019**, *132*, 425–438. [CrossRef]
62. Katoch, S.; Chauhan, S.S.; Kumar, V. A review on genetic algorithm: Past, present, and future. *Multimed Tools Appl.* **2021**, *80*, 8091–8126. [CrossRef] [PubMed]
63. Harrag, A.; Messalti, S. Extraction of Solar Cell Parameters Using Genetic Algorithm. In Proceedings of the 2015 4th International Conference on Electrical Engineering (ICEE), Boumerdes, Algeria, 13–15 December 2015; pp. 13–15.
64. Kumari, P.A.; Geethanjali, P. Adaptive Genetic Algorithm Based Multi-Objective Optimization for Photovoltaic Cell Design Parameter Extraction. *Energy Procedia* **2017**, *117*, 432–441. [CrossRef]
65. Wang, L.; Chen, Z.; Guo, Y.; Hu, W.; Chang, X.; Wu, P.; Han, C.; Li, J. Accurate Solar Cell Modeling via Genetic Neural Network-Based Meta-Heuristic Algorithms. *Front. Energy Res.* **2021**, *9*, 696204. [CrossRef]
66. Storn, R.; Price, K. Differential Evolution-A Simple and Efficient Heuristic for Global Optimization over Continuous Spaces. *J. Glob. Optim.* **1997**, *11*, 341–359. [CrossRef]
67. Luo, Q.; Peng, W.; Wu, G.; Xiao, Y. Orbital Maneuver Optimization of Earth Observation Satellites Using an Adaptive Differential Evolution Algorithm. *Remote Sens.* **2022**, *14*, 1966. [CrossRef]
68. Jiang, L.L.; Maskell, D.L.; Patra, J.C. Parameter estimation of solar cells and modules using an improved adaptive differential evolution algorithm. *Appl. Energy* **2013**, *112*, 185–193. [CrossRef]
69. Li, S.; Gu, Q.; Gong, W.; Ning, B. An enhanced adaptive differential evolution algorithm for parameter extraction of photovoltaic models. *Energy Convers. Manag.* **2020**, *205*, 112443. [CrossRef]
70. Xiong, G.; Zhang, J.; Shi, D.; Zhu, L.; Yuan, X. Parameter extraction of solar photovoltaic models via quadratic interpolation learning differential evolution. *Sustain. Energy Fuels* **2020**, *4*, 5595–5608. [CrossRef]
71. Song, Y.; Wu, D.; Wagdy Mohamed, A.; Zhou, X.; Zhang, B.; Deng, W.; Khalil, A.M. Enhanced Success History Adaptive DE for Parameter Optimization of Photovoltaic Models. *Complexity* **2021**, *2021*, 6660115. [CrossRef]
72. Parida, S.M.; Rout, P.K. Differential evolution with dynamic control factors for parameter estimation of photovoltaic models. *J. Comput. Electron.* **2021**, *20*, 330–343. [CrossRef]
73. Gao, S.; Wang, K.; Tao, S.; Jin, T.; Dai, H.; Cheng, J. A state-of-the-art differential evolution algorithm for parameter estimation of solar photovoltaic models. *Energy Convers. Manag.* **2021**, *230*, 113784. [CrossRef]
74. Wang, D.; Sun, X.; Kang, H.; Shen, Y.; Chen, Q. Heterogeneous differential evolution algorithm for parameter estimation of solar photovoltaic models. *Energy Rep.* **2022**, *8*, 4724–4746. [CrossRef]
75. Kharchouf, Y.; Herbazi, R.; Chahboun, A. Parameter's extraction of solar photovoltaic models using an improved differential evolution algorithm. *Energy Convers. Manag.* **2022**, *251*, 114972. [CrossRef]
76. Dang, J.; Wang, G.; Xia, C.; Jia, R.; Li, P. Research on the parameter identification of PV module based on fuzzy adaptive differential evolution algorithm. *Energy Rep.* **2022**, *8*, 12081–12091. [CrossRef]
77. Zhang, Y.; Wang, S.; Ji, G. A Comprehensive Survey on Particle Swarm Optimization Algorithm and Its Applications. *Math. Probl. Eng.* **2015**, *2015*, 931256. [CrossRef]
78. Dong, C.; Meng, X.; Guo, L.; Hu, J. 3D Sea Surface Electromagnetic Scattering Prediction Model Based on IPSO-SVR. *Remote Sens.* **2022**, *14*, 4657. [CrossRef]
79. Ben Hmamou, D.; Elyaqouti, M.; Arjdal, E.; Chaoufi, J.; Saadaoui, D.; Lidaighbi, S.; Aqel, R. Particle swarm optimization approach to determine all parameters of the photovoltaic cell. *Mater. Today Proc.* **2022**, *52*, 7–12. [CrossRef]
80. Ni, B.; Zou, P.; Chen, Y.; Zhang, Z. Identification of Solar Cell Model Parameters based on PSO with Adaptive Elite Mutation. In Proceedings of the 2018 Chinese Automation Congress (CAC), Xi'an, China, 30 November–2 December 2018; pp. 1340–1344.
81. Merchaoui, M.; Sakly, A.; Mimouni, M.F. Particle swarm optimisation with adaptive mutation strategy for photovoltaic solar cell/module parameter extraction. *Energy Convers. Manag.* **2018**, *175*, 151–163. [CrossRef]

82. Nunes, H.G.G.; Pombo, J.A.N.; Mariano, S.J.P.S.; Calado, M.R.A.; Felippe de Souza, J.A.M. A new high performance method for determining the parameters of PV cells and modules based on guaranteed convergence particle swarm optimization. *Appl. Energy* **2018**, *211*, 774–791. [CrossRef]
83. Rezaee Jordehi, A. Enhanced leader particle swarm optimisation (ELPSO): An efficient algorithm for parameter estimation of photovoltaic (PV) cells and modules. *Sol. Energy* **2018**, *159*, 78–87. [CrossRef]
84. Kiani, A.T.; Nadeem, M.F.; Ahmed, A.; Sajjad, I.A.; Haris, M.S.; Martirano, L. Optimal Parameter Estimation of Solar Cell using Simulated Annealing Inertia Weight Particle Swarm Optimization (SAIW-PSO). In Proceedings of the 2020 IEEE International Conference on Environment and Electrical Engineering and 2020 IEEE Industrial and Commercial Power Systems Europe (EEEIC/I&CPS Europe), Madrid, Spain, 9–12 June 2020; pp. 1–6.
85. Kiani, A.T.; Nadeem, M.F.; Ahmed, A.; Khan, I.; Elavarasan, R.M.; Das, N. Optimal PV Parameter Estimation via Double Exponential Function-Based Dynamic Inertia Weight Particle Swarm Optimization. *Energies* **2020**, *13*, 4037. [CrossRef]
86. Gao, S.; Xiang, C.; Lee, T.H. Highly Efficient Photovoltaic Parameter Estimation Using Parallel Particle Swarm Optimization on a GPU. In Proceedings of the 2021 IEEE 30th International Symposium on Industrial Electronics (ISIE), Kyoto, Japan, 20–23 June 2021; pp. 1–7.
87. Kiani, A.T.; Nadeem, M.F.; Ahmed, A.; Khan, I.A.; Alkhammash, H.I.; Sajjad, I.A.; Hussain, B. An Improved Particle Swarm Optimization with Chaotic Inertia Weight and Acceleration Coefficients for Optimal Extraction of PV Models Parameters. *Energies* **2021**, *14*, 2980. [CrossRef]
88. Fan, Y.; Wang, P.; Heidari, A.A.; Chen, H.; HamzaTurabieh; Mafarja, M. Random reselection particle swarm optimization for optimal design of solar photovoltaic modules. *Energy* **2022**, *239*, 121865. [CrossRef]
89. Karaboga, D.; Basturk, B. A powerful and efficient algorithm for numerical function optimization: Artificial bee colony (ABC) algorithm. *J. Glob. Optim.* **2007**, *39*, 459–471. [CrossRef]
90. Yan, J.; Chen, Y.; Zheng, J.; Guo, L.; Zheng, S.; Zhang, R. Multi-Source Time Series Remote Sensing Feature Selection and Urban Forest Extraction Based on Improved Artificial Bee Colony. *Remote Sens.* **2022**, *14*, 4859. [CrossRef]
91. Chen, X.; Xu, B.; Mei, C.; Ding, Y.; Li, K. Teaching–learning–based artificial bee colony for solar photovoltaic parameter estimation. *Appl. Energy* **2018**, *212*, 1578–1588. [CrossRef]
92. Wu, L.; Chen, Z.; Long, C.; Cheng, S.; Lin, P.; Chen, Y.; Chen, H. Parameter extraction of photovoltaic models from measured I-V characteristics curves using a hybrid trust-region reflective algorithm. *Appl. Energy* **2018**, *232*, 36–53. [CrossRef]
93. Xu, L.; Bai, L.; Bao, H.; Jiang, J. Parameter Identification of Solar Cell Model Based on Improved Artificial Bee Colony Algorithm. In Proceedings of the 2021 13th International Conference on Advanced Computational Intelligence (ICACI), Wanzhou, China, 14–16 May 2021; pp. 239–244.
94. Tefek, M.f.F. Artificial bee colony algorithm based on a new local search approach for parameter estimation of photovoltaic systems. *J. Comput. Electron.* **2021**, *20*, 2530–2562. [CrossRef]
95. Garoudja, E.; Filali, W. Photovoltaic Module Parameters Extraction Using Best-so-Far ABC Algorithm. In Proceedings of the 2019 International Conference on Advanced Electrical Engineering (ICAEE), Algiers, Algeria, 19–21 November 2019; pp. 1–5.
96. Duman, S.; Kahraman, H.T.; Sonmez, Y.; Guvenc, U.; Kati, M.; Aras, S. A powerful meta-heuristic search algorithm for solving global optimization and real-world solar photovoltaic parameter estimation problems. *Eng. Appl. Artif. Intell.* **2022**, *111*, 104763. [CrossRef]
97. Faris, H.; Aljarah, I.; Al-Betar, M.A.; Mirjalili, S. Grey wolf optimizer: A review of recent variants and applications. *Neural Comput. Appl.* **2017**, *30*, 413–435. [CrossRef]
98. Vinod, A.; Sinha, A.K. Estimation of parameters for one diode solar PV cell using grey wolf optimizer to obtain exact V-I characteristics. *J. Eng. Res.* **2019**, *7*, 1–19.
99. AlShabi, M.; Ghenai, C.; Bettayeb, M.; Ahmad, F.F.; El Haj Assad, M. Multi-group grey wolf optimizer (MG-GWO) for estimating photovoltaic solar cell model. *J. Therm. Anal. Calorim.* **2020**, *144*, 1655–1670. [CrossRef]
100. Xavier, F.J.; Pradeep, A.; Premkumar, M.; Kumar, C. Orthogonal Learning-Based Gray Wolf Optimizer for Identifying the Uncertain Parameters of Various Photovoltaic Models. *Optik* **2021**, *247*, 167973. [CrossRef]
101. Yesilbudak, M. Parameter Extraction of Photovoltaic Cells and Modules Using Grey Wolf Optimizer with Dimension Learning-Based Hunting Search Strategy. *Energies* **2021**, *14*, 5735. [CrossRef]
102. Ramadan, A.-E.; Kamel, S.; Khurshaid, T.; Oh, S.-R.; Rhee, S.-B. Parameter Extraction of Three Diode Solar Photovoltaic Model Using Improved Grey Wolf Optimizer. *Sustainability* **2021**, *13*, 6963. [CrossRef]
103. Zitar, R.A.; Al-Betar, M.A.; Awadallah, M.A.; Doush, I.A.; Assaleh, K. An Intensive and Comprehensive Overview of JAYA Algorithm, its Versions and Applications. *Arch. Comput. Methods Eng.* **2022**, *29*, 763–792. [CrossRef] [PubMed]
104. Yu, K.; Liang, J.J.; Qu, B.Y.; Chen, X.; Wang, H. Parameters identification of photovoltaic models using an improved JAYA optimization algorithm. *Energy Convers. Manag.* **2017**, *150*, 742–753. [CrossRef]
105. Wang, L.; Huang, C. A novel Elite Opposition-based Jaya algorithm for parameter estimation of photovoltaic cell models. *Optik* **2018**, *155*, 351–356. [CrossRef]
106. Luo, X.; Cao, L.; Wang, L.; Zhao, Z.; Huang, C. Parameter identification of the photovoltaic cell model with a hybrid Jaya-NM algorithm. *Optik* **2018**, *171*, 200–203. [CrossRef]
107. Yu, K.; Qu, B.; Yue, C.; Ge, S.; Chen, X.; Liang, J. A performance-guided JAYA algorithm for parameters identification of photovoltaic cell and module. *Appl. Energy* **2019**, *237*, 241–257. [CrossRef]

108. Luu, T.V.; Nguyen, N.S. Parameters extraction of solar cells using modified JAYA algorithm. *Optik* **2020**, *203*, 164034. [CrossRef]
109. Jian, X.; Weng, Z. A logistic chaotic JAYA algorithm for parameters identification of photovoltaic cell and module models. *Optik* **2020**, *203*, 164041. [CrossRef]
110. Zhang, Y.; Ma, M.; Jin, Z. Comprehensive learning Jaya algorithm for parameter extraction of photovoltaic models. *Energy* **2020**, *211*, 118644. [CrossRef]
111. Yang, X.; Gong, W. Opposition-based JAYA with population reduction for parameter estimation of photovoltaic solar cells and modules. *Appl. Soft Comput.* **2021**, *104*, 107218. [CrossRef]
112. Premkumar, M.; Jangir, P.; Sowmya, R.; Elavarasan, R.M.; Kumar, B.S. Enhanced chaotic JAYA algorithm for parameter estimation of photovoltaic cell/modules. *ISA Trans.* **2021**, *116*, 139–166. [CrossRef] [PubMed]
113. Saadaoui, D.; Elyaqouti, M.; Assalaou, K.; hmamou, D.B.; Lidaighbi, S. Multiple learning JAYA algorithm for parameters identifying of photovoltaic models. *Mater. Today Proc.* **2022**, *52*, 108–123. [CrossRef]
114. Jian, X.; Cao, Y. A Chaotic Second Order Oscillation JAYA Algorithm for Parameter Extraction of Photovoltaic Models. *Photonics* **2022**, *9*, 131. [CrossRef]
115. Rao, R.V.; Savsani, V.J.; Vakharia, D.P. Teaching–learning-based optimization: A novel method for constrained mechanical design optimization problems. *Comput.-Aided Des.* **2011**, *43*, 303–315. [CrossRef]
116. Chen, X.; Yu, K.; Du, W.; Zhao, W.; Liu, G. Parameters identification of solar cell models using generalized oppositional teaching learning based optimization. *Energy* **2016**, *99*, 170–180. [CrossRef]
117. Yu, K.; Chen, X.; Wang, X.; Wang, Z. Parameters identification of photovoltaic models using self-adaptive teaching-learning-based optimization. *Energy Convers. Manag.* **2017**, *145*, 233–246. [CrossRef]
118. Ramadan, A.; Kamel, S.; Korashy, A.; Yu, J. Photovoltaic Cells Parameter Estimation Using an Enhanced Teaching–Learning-Based Optimization Algorithm. *Iran. J. Sci. Technol. Trans. Electr. Eng.* **2019**, *44*, 767–779. [CrossRef]
119. Abdel-Basset, M.; Mohamed, R.; Chakrabortty, R.K.; Sallam, K.; Ryan, M.J. An efficient teaching-learning-based optimization algorithm for parameters identification of photovoltaic models: Analysis and validations. *Energy Convers. Manag.* **2021**, *227*, 113614. [CrossRef]
120. Li, L.; Xiong, G.; Yuan, X.; Zhang, J.; Chen, J. Parameter Extraction of Photovoltaic Models Using a Dynamic Self-Adaptive and Mutual- Comparison Teaching-Learning-Based Optimization. *IEEE Access* **2021**, *9*, 52425–52441. [CrossRef]
121. Mohammed, H.M.; Umar, S.U.; Rashid, T.A. A Systematic and Meta-Analysis Survey of Whale Optimization Algorithm. *Comput. Intell. Neurosci.* **2019**, *2019*, 8718571. [CrossRef]
122. Li, H.; Chang, J.; Xu, F.; Liu, Z.; Yang, Z.; Zhang, L.; Zhang, S.; Mao, R.; Dou, X.; Liu, B. Efficient Lidar Signal Denoising Algorithm Using Variational Mode Decomposition Combined with a Whale Optimization Algorithm. *Remote Sens.* **2019**, *11*, 126. [CrossRef]
123. Xiong, G.; Zhang, J.; Shi, D.; He, Y. Parameter extraction of solar photovoltaic models using an improved whale optimization algorithm. *Energy Convers. Manag.* **2018**, *174*, 388–405. [CrossRef]
124. Elazab, O.S.; Hasanien, H.M.; Elgendy, M.A.; Abdeen, A.M. Parameters estimation of single- and multiple-diode photovoltaic model using whale optimisation algorithm. *IET Renew. Power Gener.* **2018**, *12*, 1755–1761. [CrossRef]
125. Pourmousa, N.; Ebrahimi, S.M.; Malekzadeh, M.; Gordillo, F. Using a novel optimization algorithm for parameter extraction of photovoltaic cells and modules. *Eur. Phys. J. Plus* **2021**, *136*, 470. [CrossRef]
126. Peng, L.; He, C.; Heidari, A.A.; Zhang, Q.; Chen, H.; Liang, G.; Aljehane, N.O.; Mansour, R.F. Information sharing search boosted whale optimizer with Nelder-Mead simplex for parameter estimation of photovoltaic models. *Energy Convers. Manag.* **2022**, *270*, 116246. [CrossRef]
127. Xiong, G.; Zhang, J.; Yuan, X.; Shi, D.; He, Y.; Yao, G. Parameter extraction of solar photovoltaic models by means of a hybrid differential evolution with whale optimization algorithm. *Sol. Energy* **2018**, *176*, 742–761. [CrossRef]
128. Long, W.; Cai, S.; Jiao, J.; Xu, M.; Wu, T. A new hybrid algorithm based on grey wolf optimizer and cuckoo search for parameter extraction of solar photovoltaic models. *Energy Convers. Manag.* **2020**, *203*, 112243. [CrossRef]
129. Rezk, H.; Arfaoui, J.; Gomaa, M.R. Optimal Parameter Estimation of Solar PV Panel Based on Hybrid Particle Swarm and Grey Wolf Optimization Algorithms. *Int. J. Interact. Multimed. Artif. Intell.* **2021**, *6*, 145. [CrossRef]
130. Li, S.; Gong, W.; Wang, L.; Yan, X.; Hu, C. A hybrid adaptive teaching–learning-based optimization and differential evolution for parameter identification of photovoltaic models. *Energy Convers. Manag.* **2020**, *225*, 113474. [CrossRef]
131. Ndi, F.E.; Perabi, S.N.; Ndjakomo, S.E.; Abessolo, G.O. Harris Hawk Optimization Combined with Differential Evolution for the Estimation of Solar Cell Parameter. *Int. J. Photoenergy* **2022**, *2022*, 7021658. [CrossRef]
132. Yu, X.; Wu, X.; Luo, W. Parameter Identification of Photovoltaic Models by Hybrid Adaptive JAYA Algorithm. *Mathematics* **2022**, *10*, 183. [CrossRef]
133. Devarapalli, R.; Rao, B.V.; Al-Durra, A. Optimal parameter assessment of Solar Photovoltaic module equivalent circuit using a novel enhanced hybrid GWO-SCA algorithm. *Energy Rep.* **2022**, *8*, 12282–12301. [CrossRef]
134. Weng, X.; Liu, Y.; Heidari, A.A.; Cai, Z.; Lin, H.; Chen, H.; Liang, G.; Alsufyani, A.; Bourouis, S. Boosted backtracking search optimization with information exchange for photovoltaic system evaluation. *Energy Sci. Eng.* **2022**, *11*, 267–298. [CrossRef]
135. Naeijian, M.; Rahimnejad, A.; Ebrahimi, S.M.; Pourmousa, N.; Gadsden, S.A. Parameter estimation of PV solar cells and modules using Whippy Harris Hawks Optimization Algorithm. *Energy Rep.* **2021**, *7*, 4047–4063. [CrossRef]
136. Sallam, K.M.; Hossain, M.A.; Chakrabortty, R.K.; Ryan, M.J. An improved gaining-sharing knowledge algorithm for parameter extraction of photovoltaic models. *Energy Convers. Manag.* **2021**, *237*, 114030. [CrossRef]

137. Xiong, G.; Zhang, J.; Shi, D.; Yuan, X. Application of Supply-Demand-Based Optimization for Parameter Extraction of Solar Photovoltaic Models. *Complexity* **2019**, *2019*, 3923691. [CrossRef]
138. Diab, A.A.Z.; Sultan, H.M.; Aljendy, R.; Al-Sumaiti, A.S.; Shoyama, M.; Ali, Z.M. Tree Growth Based Optimization Algorithm for Parameter Extraction of Different Models of Photovoltaic Cells and Modules. *IEEE Access* **2020**, *8*, 119668–119687. [CrossRef]
139. Abbassi, R.; Abbassi, A.; Heidari, A.A.; Mirjalili, S. An efficient salp swarm-inspired algorithm for parameters identification of photovoltaic cell models. *Energy Convers. Manag.* **2019**, *179*, 362–372. [CrossRef]
140. Sharma, A.; Dasgotra, A.; Tiwari, S.K.; Sharma, A.; Jately, V.; Azzopardi, B. Parameter Extraction of Photovoltaic Module Using Tunicate Swarm Algorithm. *Electronics* **2021**, *10*, 878. [CrossRef]
141. Gupta, J.; Nijhawan, P.; Ganguli, S. Parameter extraction of solar PV cell models using novel metaheuristic chaotic tunicate swarm algorithm. *Int. Trans. Electr. Energy Syst.* **2021**, *31*, 13244. [CrossRef]
142. Ramadan, A.; Kamel, S.; Hussein, M.M.; Hassan, M.H. A New Application of Chaos Game Optimization Algorithm for Parameters Extraction of Three Diode Photovoltaic Model. *IEEE Access* **2021**, *9*, 51582–51594. [CrossRef]
143. Long, W.; Jiao, J.; Liang, X.; Xu, M.; Tang, M.; Cai, S. Parameters estimation of photovoltaic models using a novel hybrid seagull optimization algorithm. *Energy* **2022**, *249*, 123760. [CrossRef]
144. Shaban, H.; Houssein, E.H.; Pérez-Cisneros, M.; Oliva, D.; Hassan, A.Y.; Ismaeel, A.A.K.; AbdElminaam, D.S.; Deb, S.; Said, M. Identification of Parameters in Photovoltaic Models through a Runge Kutta Optimizer. *Mathematics* **2021**, *9*, 2313. [CrossRef]
145. Chellaswamy, C.; Taha; Mohammed, S.; Rajasree, R.Y.; Mohammad, J.; Gulshan, S. A Novel Optimization Method for Parameter Extraction of Industrial Solar Cells. In Proceedings of the 2019 Innovations in Power and Advanced Computing Technologies (i-PACT), Vellore, India, 22–23 March 2019; pp. 1–6.
146. Xiong, G.; Zhang, J.; Yuan, X.; Shi, D.; He, Y. Application of Symbiotic Organisms Search Algorithm for Parameter Extraction of Solar Cell Models. *Appl. Sci.* **2018**, *8*, 2155. [CrossRef]
147. Chellaswamy, C.; Ramesh, R. Parameter extraction of solar cell models based on adaptive differential evolution algorithm. *Renew. Energy* **2016**, *97*, 823–837. [CrossRef]
148. Heidari, A.A.; Mirjalili, S.; Faris, H.; Aljarah, I.; Mafarja, M.; Chen, H. Harris hawks optimization: Algorithm and applications. *Future Gener. Comput. Syst.* **2019**, *97*, 849–872. [CrossRef]